



# International Conference on High Energy Physics [online]

Deadline for Full Text Articles:

June / 24 / 2022

Deadline for Registration:

June / 30 / 2022

**6 - 7 July , 2022**

School of Physics  
Damghan University, Damghan, Iran

<https://www.skyroom.online/ch/iybssd2022/ichep1>

## »» Topics:

## »» Keynote Speakers:

- Prof. Salvatore Capozziello
- Prof. Ramon Herrera
- Prof. Hassan Firouzjahi
- Prof. Yasaman Farzan
- Prof. Seyed Mahmoud Sadat Kiai
- Prof. Javad Rahighi
- High Energy Physics - Theory
- High Energy Physics - Phenomenology
- High Energy Physics - Experiment
- High Energy Physics - Lattice
- Mathematical Physics
- Quantum Physics
- General Relativity and Quantum Cosmology
- Nuclear Theory
- Nuclear Experiment- Fusion and Fission

🌐 [hep.du.ac.ir](http://hep.du.ac.ir)

✉ [hep2022@du.ac.ir](mailto:hep2022@du.ac.ir), [hep2022du@gmail.com](mailto:hep2022du@gmail.com)

★ The selected papers will be published by JHAP



## Scientific Committee

- Prof. Anne Taormina (Durham University, UK)
- Prof. Jafar Sadeghi (Mazandaran University, Iran) [Chairman]
- Prof. İzzet Sakallı (Eastern Mediterranean University, Turkey)
- Prof. Mario C. Rocca (Universidad Nacional de La Plata, Argentina)
- Prof. A. Ghasemizad (Guilan University, Iran)
- Prof. Hadi Hadizade Yazdi (Ferdowsi University, Iran)
- Dr. Sudhaker Upadhyay (K. L. S. College, India)
- Dr. Nahid Ahmadi (Tehran University, Iran)
- Dr. Nima Ghal-eh (Ferdowsi University, Iran)
- Dr. Mohsen Dehghani (Razi University, Iran)
- Dr. Haidar Sheikh-Ahmadi (North-West University, South Africa)
- Dr. Behnam Pourhassan (Damghan University, Iran)
- Dr. Hoda Farahani (Damghan University, Iran)
- Dr. Babak Khanbabaie (Damghan University, Iran)
- Dr. Leila Shahkarami (Damghan University, Iran)
- Dr. Ahmad Naghidokht (Damghan University, Iran)

## **Executive Committee**

- **Dr. Babak Khanbabai (Damghan University, Iran) [Chairman]**
- **Dr. Behnam Pourhassan (Damghan University, Iran)**
- **Dr. Mehdi Shokri (Tehran University, Iran)**
- **Mr. Morteza Tavakkoli (Damghan University, Iran)**
- **Dr. Shahab Shahidi (Damghan University, Iran)**

## Table of Contents

<b>Part One: Keynote Speakers</b> .....	<b>1</b>
Reconstructing Inflation (R. Herrera).....	2
The Gravitational Energy-Momentum Pseudo-Tensor in Higher Order Theories of Gravity (S. Capozziello).....	3
Stochastic inflation and cosmological perturbations (H. Firouzjahi).....	4
Searching for new physics by forward experiments (Y. Farzan).....	5
Nuclear fusion technology as a future energy solution (S. M. Sadat Kiai).....	6
Iranian Light Source Facility, the first Iranian experience in establishing large scale science facilities in Iran (J. Rahighi).....	7
<b>Part two: Invited Talks</b> .....	<b>8</b>
$4D$ Gauss–Bonnet massive black hole and their thermodynamics (S. Upadhyay).....	9
Ultraviolet Finiteness or Asymptotic Safety in Higher Derivative Gravitational Theories (R. Leslaw).....	10
The Higgs boson as a self-similar system (M. Ahmadvand).....	11
Holographic dark energy inspired from the cubic curvature invariant (R. Prabir).....	12
Kinks, vortices and monopoles (B. Dionisio).....	13
Dissecting the Hubble constant tension in extended cosmologies (E. R. Celia).....	14
<b>Part three: Oral presentations</b> .....	<b>15</b>
Gravitational slip parameter and Gravitational Waves in Modified Gravity theories (M. Ranjbar).....	16
Investigation of Stability Zones for Internal Kink Mode in IR-T1 Tokamak (A. Naghidokht).....	22
Hawking Radiation for Hayward Black hole in Einstein–Gauss–Bonnet Gravity through Tunneling Process (S. Shahraini).....	29
Modified AdS/QCD model in an external electric field (L. Shahkarami).....	35
Quantum Correction to the Black Holes Thermodynamics (B. Pourhassan).....	40
AdS/BCFT correspondence and BTZ black hole within electric field (F. F. Santos).....	44
<b>Part four: Poster presentations</b> .....	<b>45</b>

Travelling wave solution of Balitsky-Kovchegov equation (R. Saikia).....	46
Dirac particle near R - N black hole, quasinormal mode and harmonic oscillator energy (M. Alipour).....	53
Constant-roll inflation in the deformed phase space scenario (S. Noori Gashti).....	58
Color Reconnection Modelling in PYTHIA8 (N. Firdous).....	63

# Part one

## Keynote Speakers

# Reconstructing Inflation

Ramon Herrera

*Instituto de Física, Pontificia Universidad Católica de Valparaíso, Valparaíso, Chile*

## **Abstract:**

The reconstruction of an inflationary universe in the context of different theories of gravitation, considering as attractors the scalar spectral index and the tensor to scalar ratio as a function of the number of e-folding is studied. Also, we study in great detail the analytical and exact solutions for the cosmological perturbations together with the corresponding reconstruction of the background variables but from the perturbation equation (Mukhanov-Sasaki eq.). To apply the unification in our model, we consider some examples from these methodologies in order to rebuild the effective potential and another coupling parameter as a function of the inflation field. Thus, in this presentation we show that it is possible to unify the theoretical foundations and the observational parameters corroborated by observations, in the reconstruction of an early universe.

Wednesday 6th July 2022

# The Gravitational Energy-Momentum Pseudo-Tensor in Higher Order Theories of Gravity

S. Capozziello

*Dipartimento di Scienze Fisiche, Università di Napoli, Italy*

## **Abstract:**

We discuss the generalization of gravitational energy-momentum pseudo-tensor to Extended Theories of Gravity, in particular to higher-order theories in curvature invariants. This result is achieved by imposing that the local variation of gravitational action of any order  $n$  vanishes under rigid translations. We also prove that this tensor, in general, is not covariant but only affine, that is, it is a pseudo-tensor. The pseudo-tensor is calculated in the weak-field limit up to a first non-vanishing term of order  $h^2$ , where  $h$  is the metric perturbation. The average value of the pseudo-tensor, over a suitable spacetime domain, is obtained. Finally, we calculate the emitted power, per unit solid angle, carried by a gravitational wave in a direction  $x$  for a fixed wave number  $k$  under a suitable gauge.

Wednesday 6th July 2022

# Stochastic inflation and cosmological perturbations

Hassan Firouzjahi

*School of Astronomy, Institute for Research in Fundamental Sciences (IPM), Tehran, Iran*

## **Abstract:**

We review the formalism of stochastic inflation and its applications in cosmological perturbation theory. We employ the stochastic formalism to calculate the correlation functions of cosmological perturbations such as the power spectrum and bispectrum. Some applications of stochastic formalism to the first passage time for Brownian motion in the dS background is reviewed.

Thursday 7th July 2022

# Searching for new physics by forward experiments

Yasaman Farzan

*School of physics, Institute for Research in Fundamental Sciences (IPM), Tehran, Iran*

## **Abstract:**

Despite the hopes and the excellent experimental performance, the main detectors of the LHC, CMS and ATLAS, have not discovered any new elementary particle so far. The search is however ongoing. It is conceivable that new physics involves light feebly-interacting particles that are emitted in the forward direction beyond the angular reach of these detectors. There is a rich program of forward experiments which can test such models. In this talk, I will discuss the potential of FASER $\nu$  and SND@LHC experiments in searching for new physics.

Thursday 7th July 2022

# Nuclear fusion technology as a future energy solution

S. M. Sadat Kiai

*Nuclear Science Research School, Nuclear Science & Technology Research Institute (N.S.T.R), Tehran, Iran*

## **Abstract:**

Fossil fuel consumption is still rising each year and harming our environment. With the current rate of consumption without finding additional reserves, there will be a time, perhaps measured in decades, generation of energy from fossil fuels will run out. However, in the future the way we produce energy is certainly not from fossil fuels but from our knowledge. Nuclear fusion energy offers the prospect of an almost inexhaustible and carbon free source of energy for future generations.

Thursday 7th July 2022

## Iranian Light Source Facility, the first Iranian experience in establishing large scale science facilities in Iran.

Javad Rahighi

*Iranian Light Source Facility (ILSF), Institute for Research in Fundamental Science (IPM), Tehran, Iran*

### **Abstract:**

Higher education in Iran has been developing at tremendous speed and capacity since early 1970's. A sharp increase in the number of universities & students in Iran (as well as no of Iranian students in Europe & US) in 1980's followed by increasing Limitation for Iranian Scientists & Students to access laboratories and research centers in Europe and the US. In the early 2000 while the engine of higher education was in action to generate graduates in millions, the lack of investment deprived universities of having the necessary research tools and equipment. At the international level, some very limited advances were made. Iran joined CERN in 2001 and SESAME, Synchrotron-light for Experimental Science and applications in the Middle East, in 2004. Under these circumstances, Iran decided to build a large-scale science national laboratory. Such science facility will have a great impact on developing human capital and creating spinout firms to commercially exploit new knowledge and technology. The Iranian Light Source Facility Project (ILSF) is a 4th generation light source with energy of 3 GeV, a full energy injector and a 150 MeV linac as pre-injector. The stored beam current in top up mode is 400 mA, the beam lifetime is about 7 h, and the average pressure of vacuum chamber is approximately  $1.33 \times 10^{-7}$  Pa (1 nTorr). The ILSF storage ring is a very low emittance (270 pm-rad) ring, has been designed to be competitive in the future operation years.

Thursday 7th July 2022

## Part two

# Invited Speakers

# 4D AdS Gauss--Bonnet massive black hole and their thermodynamics

Sudhaker Upadhyay

*Department of Physics, K. L. S. College, Nawada, India*

Abstract:

We obtain a black hole solution for 4D AdS Einstein-Gauss-Bonnet massive gravity and discuss their thermodynamical properties by insuring the validity of the first-law of thermodynamics and the Smarr relation. Furthermore, we discuss the stability and phase transition of the model.

Thursday 7th July 2022

# Ultraviolet Finiteness or Asymptotic Safety in Higher Derivative Gravitational Theories

Rachwal Leslaw

*Departamento de Física, Instituto de Ciências Exatas, Universidade Federal de Juiz de Fora, Juiz de Fora  
33036-900, MG, Brazil*

## **Abstract:**

We present and discuss well known conditions for ultraviolet finiteness and asymptotic safety. The requirements for complete absence of ultraviolet divergences in quantum field theories and existence of a non-trivial fixed point for renormalization group flow in the ultraviolet regime are compared based on the example of a six-derivative quantum gravitational theory in  $d=4$  spacetime dimensions. In this model, it is possible for the first time to have fully UV-finite quantum theory without adding matter or special symmetry, but by inclusion of additional terms cubic in curvatures. We comment on similarities and some apparent differences between the two approaches, but we show that they are both compatible to each other. Finally, we motivate the claim that actually asymptotic safety needs UV-finite models for providing explicit form of the ultraviolet limit of Wilsonian effective actions describing special situations at fixed points.

Wednesday 6th July 2022

# The Higgs boson as a self-similar system

Moslem Ahmadvand

*School of Physics, Institute for Research in Fundamental Sciences (IPM), P. O. Box 19395-5531, Tehran,  
Iran*

## **Abstract:**

I propose a new solution to the hierarchy (naturalness) problem, concerning quantum corrections of the Higgs mass. Suggesting the Higgs boson as a system with a self-similar internal structure, I obtain its two-point function and find that the quadratic divergence is replaced by a logarithmic one. It is shown that the partonic-like distribution follows the Tsallis statistics and also high energy physics experimental data for the Higgs transverse momentum distribution can be described by a self-similar statistical model.

Thursday 7th July 2022

## Holographic dark energy inspired from the cubic curvature invariant.

Rudra Prabir

*Department of Mathematics, Asutosh College, Kolkata-700026, India*

### **Abstract:**

A model of holographic dark energy is proposed which is inspired by the cubic curvature invariant formed by the contraction of three Riemann tensors. A combination of Ricci scalar and the cubic invariant is used to describe the infrared cutoff of the holographic dark energy. Such a construction is extremely useful since evolution does not depend on the past or future features of the universe, but completely on its present features. Moreover, the use of invariants makes the theory more fundamental. The model is constructed and its cosmological features are examined. The analytical solutions of various cosmological parameters such as the density parameter, equation of state parameter, and deceleration parameter are extracted and their behavior is studied. It is seen that the holographic dark energy model can exhibit the entire thermal history of the universe, sequentially starting from radiation in the early universe, followed by matter, and finally the dark energy dominated epoch at late times. The equation of state parameter shows that the model can exhibit quintessence nature, phantom-divide crossing, and even phantom nature depending on the choice of parameter spaces.

Wednesday 6th July 2022

## Kinks, vortices and monopoles

Dionisio Bazeia

*Departamento de Física, Universidade Federal da Paraíba, C.P. 5008, 58051-970 João Pessoa PB, Brazil*

### **Abstract:**

In this talk we review the basic features of kinks, vortices and monopoles, and investigate new possibilities, described under the presence of extra symmetries and modifications in some physical properties of the corresponding medium. We study, in particular, multikinks, multilayered vortices, and magnetic monopoles with core and shell structures.

Thursday 7th July 2022

# Dissecting the Hubble constant tension in extended cosmologies

Escamilla Rivera Celia

Instituto de Ciencias Nucleares, Universidad Nacional Autonoma de Mexico, Circuito Exterior C.U., A.P.  
70-543, Mexico D.F. 04510, Mexico.

## **Abstract:**

The current cosmological probes have provided an extraordinary confirmation of the standard  $\Lambda$ CDM cosmological model, that has been constrained with unprecedented accuracy. However, with the increase of the experimental sensitivity a few statistically significant tensions between different independent cosmological datasets emerged. While these tensions can be in portion the result of systematic errors, the persistence after several years of accurate analysis strongly hints at cracks in the standard cosmological scenario and the need for new physics. In this talk I will list a few interesting new cosmological models in the direction of extended theories of gravity that could solve this tension and discuss how the new computational techniques will be crucial in this role.

Wednesday 6th July 2022

## Part three

# Oral Presentations

## Gravitational slip parameter and Gravitational Waves in Modified Gravity theories

Maryamalsadat Ranjbar<sup>1</sup>, Siamak Akhshabi<sup>2</sup>, Mohsen Shadmehri<sup>3</sup>

<sup>1</sup>Graduate student, Golestan University, Gorgan, Iran.

Email: m.ranjbar98@stu.gu.ac.ir

<sup>2</sup>Assistant Professor, Golestan University, Gorgan, Iran.

Email: s.akhshabi@gu.ac.ir

<sup>3</sup> Associated Professor, Golestan University, Gorgan, Iran.

Email: m.shadmehri@gu.ac.ir

**Abstract.** Despite the discovery of late-time accelerated expansion of the universe, we still have no clue about the physics behind that. Therefore, the answer might be in Modified Gravity theories. In this research, we study the gravitational slip parameter in the context of theories including torsion, such as Einstein-Cartan theory to test the possible modification to standard General relativity.

Keywords: Einstein-Cartan Theory, Gravitational Slip Parameter, Modified Gravity.

### 1 Introduction

Discovering the expansion of the universe convinced Einstein that the existence of Cosmological constant in his field equations is unnecessary. However, with the recent discovery of accelerated expansion of the universe, it is no longer possible to neglect the role of this term from his equations. The Cosmological constant which has a very small constant density and negative pressure, could be an appropriate candidate for explaining accelerated expansion. However, when trying to explain the Cosmological constant as the zero-point energy, a serious controversy arises; there is a major difference in order of 120, between the observed value for the Constant from Cosmology and the theoretical estimated value from Quantum Field Theory.

The limitations of General Relativity in understanding the accelerated expansion of the universe and some other phenomena have caused some scientists to consider the possibility that the theory of General Relativity may not be a completely correct theory for studying the universe and it may be a branch of a more comprehensive theory.[1][2]

### Einstein-Cartan Theory

In order to expand the validity of the theory of gravitation to microphysics, it is essential to consider the spin angular momentum of matter. By adding spin angular momentum to energy-momentum Tensor, a quantity related to rotation must also be added to the geometric part of the field equations. This quantity is known as torsion.

In this case, the resulting geometry of space-time is no longer Riemannian, but is a slightly more general space-time, the 4-dimensional Riemann-Cartan space-time. The simplest theory with this type of generalization of general relativity is called Einstein-Cartan (EC) theory of gravity [3].

The action of Einstein-Cartan theory is:

$$S = \frac{1}{2\kappa} \int d^4x \mathcal{R} + \int d^4x \mathcal{L}_m \quad (1)$$

Which  $\mathcal{R}$  is the Ricci scala constructed from full connection and  $\mathcal{L}_m$  is matter Lagrangian. To obtain the field equation in the Einstein-Cartan theory, we start with the definition of metric and connection. In this paper we assume a flat FRW universe with the metric signature  $(+, -, -, -)$ .

$$ds^2 = dt^2 - 2a(t)\gamma_{ij}dx^i dx^j, \quad (2)$$

$$\Gamma_{\mu\nu}^\alpha = \bar{\Gamma}_{\mu\nu}^\alpha - K_{\mu\nu}^\alpha, \quad (3)$$

$\bar{\Gamma}_{\mu\nu}^\alpha$  is the standard Christoffel connection and  $K_{\mu\nu}^\alpha$  is the contortion tensor, related to torsion by:

$$K_{\mu\nu}^\alpha = -S_{\mu\nu}^\alpha + S_{\nu\mu}^\alpha - S^\alpha_{\mu\nu} = -K_{\mu\nu}^\alpha, \quad (4)$$

$S_{\mu\nu}^\alpha$  is the Torsion tensor which is the antisymmetric part of the connection:

$$S_{\mu\nu}^\alpha = \Gamma_{[\mu\nu]}^\alpha = \frac{1}{2}(\Gamma_{\mu\nu}^\alpha - \Gamma_{\nu\mu}^\alpha), \quad (5)$$

And the field equation will be

$$\bar{G}_{\mu\nu} = \bar{R}_{\mu\nu} - \frac{1}{2} g_{\mu\nu} \bar{R} = \kappa \tilde{\sigma}_{\mu\nu}. \quad (6)$$

Where

$$\tilde{\sigma}_{\mu\nu} := \sigma_{\mu\nu} + \kappa \left\{ \begin{array}{l} -4 \tau_{\mu\lambda}^{[\alpha} \tau_{\nu\alpha}^{\lambda]} - 2 \tau_{\mu\lambda\alpha} \tau_{\nu}^{\lambda\alpha} + \tau_{\alpha\lambda\mu} \tau^{\alpha\lambda}_{\nu} + \\ \frac{1}{2} g_{\mu\nu} \left( 4\tau_{\lambda}^{\beta}{}_{[\alpha} \tau^{\lambda\alpha}{}_{\beta]} + \tau^{\alpha\lambda\beta} \tau_{\alpha\lambda\beta} \right) \end{array} \right\}. \quad (7)$$

Notice that  $\tau_{\alpha\lambda\beta}$  is the Spin tensor,  $\tilde{\sigma}_{\mu\nu}$  is the energy-momentum tensor in Einstein-Cartan theory and  $\sigma_{\mu\nu}$  is the standard energy-momentum tensor in General Relativity [4].

By considering symmetries of FRW space-time, the only non-zero component of the spin tensor are [8]:

$$\tau_{011} = \tau_{022} = \tau_{033} = -\tau_{A0A} = q(t), \quad (8)$$

Assuming a perfect fluid for the standard energy-momentum tensor, Friedman equation in Einstein-Cartan theory is:

$$3 \left( \frac{\dot{a}}{a} \right)^2 = \kappa \rho(t) + 3 \kappa^2 a(t)^{-4} q(t)^2. \quad (9)$$

### Gravitational Slip, A Model Independent Parameter

A modification in geometric structure of space-time causes noticeable differences in gravitational waves equation compared to the known form of gravitational waves in general relativity.

Various gravity theories have two general phenomenological effects at the level of linear and scalar perturbation:

- A modification of the strength of gravity at large scales
- An alteration of the weak gravitational lensing effect

Measurement of the two aforementioned effects allows us to obtain gravitational slip parameter  $\eta$ ; which is the ratio of two scalar gravitational potentials (scalar metric fluctuations):

$$\eta = \Phi/\Psi. \quad (10)$$

The existence of gravitational slip parameter ( $\eta \neq 1$ ) in the presence of perfect fluid matter is a clue of a modification in gravity. In addition, this parameter is a model independent quantity which distinguishes the groups of gravity models. [5-7]

### Gravitational Slip Parameter in Einstein-Cartan Theory

We intend to investigate Gravitational Slip parameter for the first time in gravitational theories including torsion, such as Einstein-Cartan theory. We start by obtaining scale factor and spin tensor as a function of time for various different matter content for the universe.

By inserting equation (7) and (8) into equation (6), the {00} and {ij} component of the field equations are obtained as:

$$3 \left( \frac{\dot{a}(t)}{a(t)} \right)^2 = \kappa \rho(t) + 3 \kappa^2 a(t)^{-4} q(t)^2. \quad (11)$$

$$- \left( 2 \frac{\ddot{a}(t)}{a(t)} + \left( \frac{\dot{a}(t)}{a(t)} \right)^2 \right) a^2(t) \gamma_{ij} = (\kappa a(t)^2 P(t) - 2 \kappa^2 a(t)^{-4} q(t)^2) \delta_{ij}. \quad (12)$$

Where  $a(t), q(t), \rho(t), P(t)$  are Scale Factor, Spin density, Energy density and pressure respectively. Also consider that  $P(t) = \omega \rho(t)$  and  $\rho(t) = \frac{\rho_0}{a(t)^{3(1+\omega)}}$  for a single component universe. By solving system of equations (11) and (12), the scale factor and spin can be obtained:

$$q(t) = \frac{-\sqrt{9 \dot{a}(t)^2 a(t)^2 - 3 \kappa \rho_0 a(t)}}{3 \kappa}. \quad (13)$$

$$a(t) = \text{Root of} \left( \int^Z \frac{-3x}{\sqrt{x^3 + \kappa \rho_0}} dx + t \right). \text{ (Radiation dominated)} \quad (14)$$

$$a(t) = \text{Root of} \left( \int^Z \frac{x\sqrt{3}}{\sqrt{x(x^2 + \kappa \rho_0)}} dx + t \right). \text{ (Matter dominated)} \quad (15)$$

Then we can estimate a specific solution such as  $\alpha t^\beta$ , for the system of equations (9 and 10) where  $\alpha$  and  $\beta$  are two constants. We test the ansatz by directly substituting it into the system of equations. "Fig. 1" and "Fig. 2", show the behavior of the fitted ansatz and numerical solution to the integrals (14) and (15). The values of constants  $\alpha$  and  $\beta$  can be deduced by fitting an appropriate curve to the numerical solution, the results for  $a(t)$  and  $q(t)$  are:

$$a(t) = 6.01 (t)^{\frac{1}{2}-0.001}. \text{ (Radiation dominated)} \quad (16)$$

$$a(t) = 2.98 (t)^{\frac{2}{3}-0.134}. \text{ (Matter dominated)} \quad (17)$$

$$q(t) = -0.1^{42} (t)^{\frac{1}{3}-(0.268)}. \text{ (Matter dominated)} \quad (18)$$

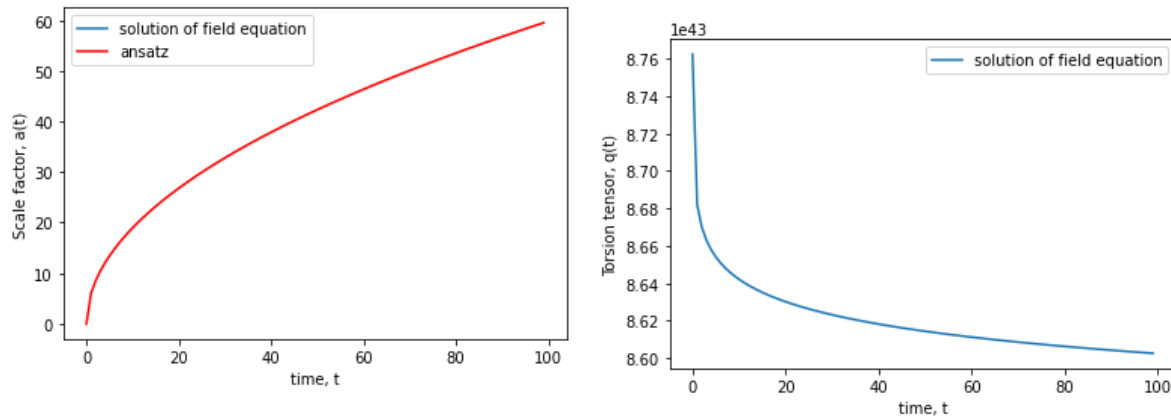


Figure 1. ansatz of scale factor behaves exactly same as solution (left), behavior of torsion over time (right); radiation dominated area.

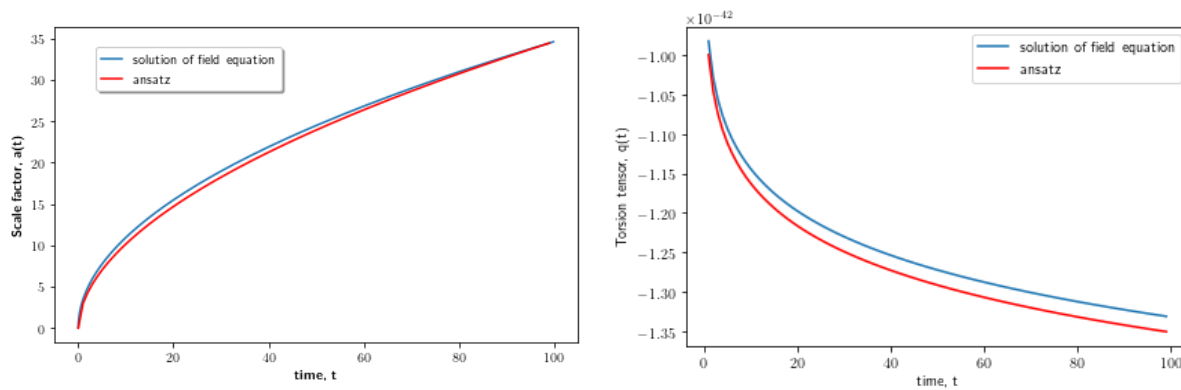


Figure 2. ansatz of scale factor (left) and torsion (right) behave same as solution.

Now we can analyze the scalar metric fluctuation  $(\Phi(t), \Psi(t))$ , by perturbation of field equations.

We assume the metric fluctuation as follow<sup>1</sup>:

$$g_{\mu\nu} + \delta g_{\mu\nu} = \begin{pmatrix} 1 + 2\Psi & 0 \\ 0 & -a^2(t) + 2\Phi a(t)^2(t) \delta_{ij} \end{pmatrix}. \quad (19)$$

The Spin density perturbation in this case is not first order and we neglect it here.

Performing standard Fourier transformation of scalar perturbation parameters, the perturbed field equation of Einstein-Cartan will be obtained as follows

$$3H(t)^2 - 2k^2\Phi(t) - 6H(t)\dot{\Phi}(t) = \kappa [\rho(t) + \delta\rho(t) + 2\rho(t)\Psi(t)] + \kappa^2 [3a(t)^{-4}q(t)^2 + 12a(t)^{-4}q(t)^2\Phi(t) + 6a(t)^{-4}q(t)^2\Psi(t)]. \quad (20)$$

$$2k(\dot{\Phi}(t) + H(t)\Psi(t)) = 0. \quad (21)$$

$$\begin{aligned} & \left[ -2\left(\frac{\ddot{a}(t)}{a(t)} + \left(\frac{\dot{a}(t)}{a(t)}\right)^2\right) - \left(\frac{\dot{a}(t)}{a(t)}\right)^2 - k^2(\Psi(t) + \Phi(t)) + \left(4\frac{\ddot{a}(t)}{a(t)} + 4\left(\frac{\dot{a}(t)}{a(t)}\right)^2 + 2\left(\frac{\dot{a}(t)}{a(t)}\right)^2\right)(\Phi(t) + \right. \\ & \left. \Psi(t)) + 2\ddot{\Phi}(t) + 2H(t)\dot{\Psi}(t) + 4H(t)\dot{\Phi}(t) \right] \delta_{ij} + k^2(\Psi(t) - \Phi(t)) = \kappa a(t)^2 [P(t) + \delta P(t) - 2P(t)\Phi(t)] \delta_{ij} + \kappa^2 a(t)^{-2} q(t)^2 [22\kappa^2 a(t)^{-2} q(t)^2 \Psi(t) - \\ & 52\kappa^2 a(t)^{-2} q(t)^2 \Phi(t) - 62\kappa^2 a(t)^{-2} q(t)^2] \delta_{ij}. \quad (22) \end{aligned}$$

Where,  $\mathbf{k}$  is the wave-number.

## Results and Discussion

We solved the system of equations (20, 21, 22) and illustrate the value of Gravitational slip parameter over time in "Fig. 3" and "Fig. 4":

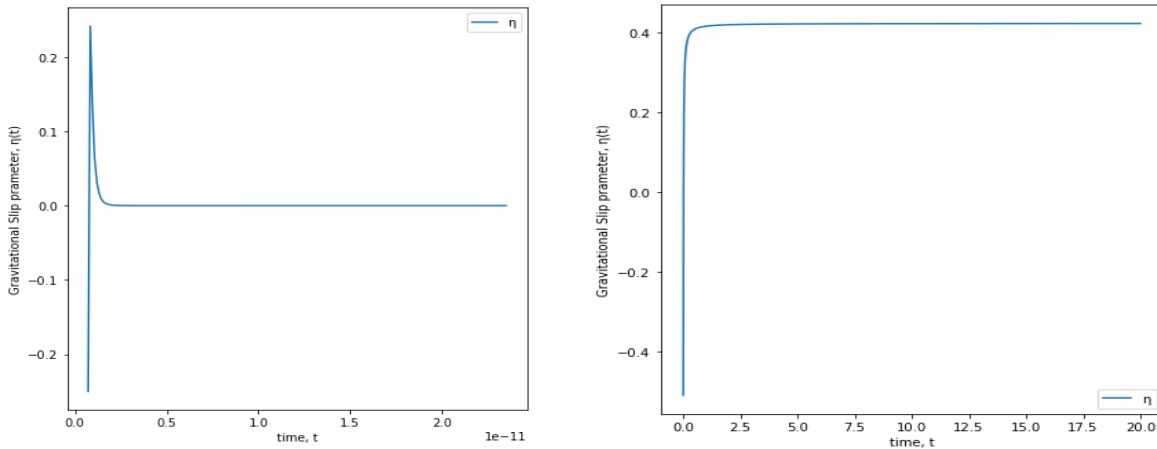


Figure3. Illustrate the value of  $\eta$  in radiation-dominated area(left)

<sup>1</sup> We consider Newtonian gauge,  $B=E=0$

Figure4. Shows the value of  $\eta$  in matter-dominated area(right)

As can be seen from "Fig. 3" and "Fig. 4", the value of Gravitational slip parameter in presence of perfect fluid is not equal to  $\eta = 1$  for various redshifts. Also, the Slip parameter obtained from Einstein-Cartan theory is perfectly match with observed values shown in "Table 1" [10].

Redshift	$Z_1= 0.296$	$Z_2= 0.58$	$Z_3=0.86$
Slip parameter	$0.57 \pm 1.05$	$0.48 \pm 0.96$	$-0.11 \pm 3.21$

**Table 1.** Observed values of slip parameter  $\eta$  for different redshifts.

The results show in each case the predicted values of  $\eta$  in Einstein-Cartan theory lies within the observed range in each redshift, however a more comprehensive study is needed to distinguish between EC results and other modified gravity theories.

## References

- [1] Barbara Ryden, "Introduction to Cosmology", Addison Wesley, 1st edition
- [2] L. Amendola and S. Tsujikawa, "Dark Energy: Theory and Observations", Cambridge University Press, 2010.
- [3] F. W. Hehl, P. Von Der Heyde, G. D. Kerlick and J. M. Nester, "General Relativity with Spin and Torsion: Foundations and Prospects", Rev. Mod. Phys. 48, 393; 1976.
- [4] S. Bravo Medina, M. Nowakowski and D. Batic, "Einstein-Cartan Cosmologies", *Annals Phys.* 400, 64; 2019.
- [5] L. Amendola, M. Kunz, M. Motta, I. D. Saltas, and I. Sawicki, "Observables and unobservables in dark energy cosmologies," Phys.Rev., vol. D87, p. 023501, 2013.
- [6] M. Motta, I. Sawicki, I. D. Saltas, L. Amendola, and M. Kunz, "Probing Dark Energy through Scale Dependence," Phys.Rev., vol. D88, p. 124035, 2013.
- [7] Ippocratis D. Saltas, Luca Amendola, Martin Kunz, Ignacy Sawicki, "Modified gravity, gravitational waves and the large-scale structure of the Universe: A brief report ", Based on a talk given at the 15th Marcel Grossmann meeting, 2018.
- [8] H. Goenner and F Muller-Hoissen, "Spatially homogeneous and isotropic spaces in theories of gravitation with torsion", *Quantum Grav.* 1. 651-672.; 1984.
- [9] Daniel Baumann, "Cosmology, part III Mathematical Tripos", Cambridge University Press, Chapter4; 2022.
- [10] A. M. Pinho, S. Casas, and L. Amendola, "Model-independent reconstruction of the linear anisotropic stress  $\eta$ ", *JCAP*, vol. 1811, no. 11, p. 027, 2018.

## Investigation of Stability Zones for Internal Kink Mode in IR-T1 Tokamak

Fatemeh Nabizadeh, Ahmad Naghidokht  
School of Physics, Damghan University, Damghan, Iran.  
Email: fatemeh Nabizadeh98@gmail.com  
Email: ahmadnaghidokht@gmail.com

**Abstract.** Internal kink mode has been considered as an effective factor in disruptions and according to this issue, its stability in IR-T1 tokamak (circular cross-section plasma) has been investigated. Tokamak plasma stabilization against this mode is provided by a suitable profile for the safety factor. By considering a common profile for toroidal current density, corresponding profiles for the safety factor and growth rate of the internal kink instability were obtained for IR-T1 tokamak. The results show the highest stability in the plasma boundary regions for all  $\nu$  values and the highest instability in the central plasma regions for values of  $\nu > 3$ . Also, comparing between these results with the findings of data fitting with one of the main codes in the field of this instability, shows a good agreement for the order of growth rate of instability.

**Keywords:** Magnetohydrodynamic stability, Safety factor, Internal kink mode, IR-T1 tokamak.

### 1 Introduction

Plasma instability remains a major obstacle to the magnetic confinement fusion approach in a nuclear reactor, especially large-scale magnetohydrodynamic (MHD) modes that can have the most destructive effects on stability. The role of the ideal MHD model is to study the equilibrium and stability properties of different structures for the continuous operation of nuclear fusion energy extraction structures, especially magnetic fusion energy. Even if the magnetic field settings of the structures are in accordance with the ideal MHD theory, perturbation is still possible, so achieving MHD stability is essential. Non-ideal effects such as limited resistance, thermal conductivity and viscosity may lead to instabilities that are weaker than what is allowed by the ideal MHD [1,2]. Anyway, the turbulence caused by MHD instabilities can be in any form, but the resonance will occur for instabilities that have surfaces with definite  $q = \frac{m}{n}$  and produce certain modes of instability. The numbers  $m$  and  $n$  are used to indicate the poloidal and the toroidal mode. The stability of the tokamak plasma in these modes is provided by the safety factor  $q$  [3, 4].

Kink modes lead to convexity and concavity in magnetic field lines, resulting in their fracture. This is followed by magnetic islands, which destroy the stability of the magnetic flux lines and cause the plasma to become unstable. Internal kink mode ( $n = 1, m = 1$ ) is considered as a direct cause or at least an important component in the dynamics of sawtooth oscillations in tokamak, which causes disruptions and consequently catastrophic loss of plasma control [5, 6]. The growth

rate of this mode depends to a large extent on the  $q$  profile, so that a very small change in  $q$  may destabilize the stable equilibrium. Analytical and numerical calculations related to the growth rate in the ideal and the resistance mode in TCV tokamak [7, 8] have studied these effects. In an NSTX species plasma, internal kink has been investigated in the presence of pure toroidal flow [9]. This mode is also one of the MHD instabilities in common discharge scenarios in ASDEX-U tokamak [10,11]. Studies related to this magnetohydrodynamic mode and its stability have also been performed in Damavand tokamak [12]. In this work, we will study the stability regions for the internal kink mode in IR-T1 tokamak, a small ohmic tokamak with an air core, copper-free shell, and circular cross-section plasma.

## 2 The Growth Rate of Internal Kink Instability

The basic variable characterizing stability,  $q(r)$ , is related to the toroidal current distribution. Radial profile of the safety factor  $q(r)$  usually has its minimum value inside or near the magnetic axis and increases outwards. At high aspect ratio and circular cross section plasma, the behavior is simply determined as follows:

$$q(r) = \frac{2\pi r^2 B_\phi}{\mu_0 R_0 I_p} = \frac{r B_\phi}{R_0 B_\theta} \quad (1)$$

Where  $B_\phi$ ,  $B_\theta$ ,  $R_0$  and  $I_p$  are toroidal field, poloidal field, major radius and plasma current, respectively. For the following current distribution ( $a$  is minor radius of plasma and  $\nu = 1,2,3,4,5$ ):

$$j_\phi(r) = j_{\phi 0} \left(1 - \frac{r^2}{a^2}\right)^\nu \quad (2)$$

Next, using Maxwell equations, the poloidal magnetic field profile is given as:

$$B_\theta = \frac{\mu_0 j_\phi(0) a^2}{2(\nu+1)r} \left(1 - \left(1 - r^2/a^2\right)^{\nu+1}\right) \quad r \leq a$$

$$B_\theta = \frac{\mu_0 j_\phi(0) a^2}{2(\nu+1)r} \quad a < r < b \quad (3)$$

Finally, the radial profile of the safety factor will be obtained from Eq. (1) [13]:

$$q(r) = \frac{2\pi a^2}{\mu_0 I_p} \frac{B_\phi r^2/a^2}{R_0 \left[1 - \left(1 - r^2/a^2\right)^{\nu+1}\right]} \quad (4)$$

We are now looking to calculate the growth rate of internal kink instability. For this purpose, we will consider a very simple zero pressure cylindrical equilibrium with nearly constant current in the  $z$  direction. The plasma is contained in the region  $r < a$  and the wall at  $r = b$  is considered perfectly conducting. The region between  $r = a$  and  $r = b$  is the vacuum region. The magnetic field is obtained as follows:

$$\mathbf{B}_0 = (B_0 + B_z(r))\hat{\mathbf{z}} + \mathbf{B}_\theta(r) \quad (5)$$

Where  $\mathbf{B}_0$  is the dominant toroidal field in a tokamak and  $r$  is radius of the cylinder. Pushing the plasma a small distance away from its equilibrium state, the momentum equation becomes:

$$\rho_0 \frac{\partial^2 \boldsymbol{\xi}}{\partial t^2} = \mathbf{J}_0 \times \delta \mathbf{B} + (\nabla \times \delta \mathbf{B}) \times \mathbf{B}_0 = \mathbf{F}(\boldsymbol{\xi}) \quad (6)$$

Where  $\boldsymbol{\xi}$  and  $\rho_0$  are the plasma displacement ( $\partial \boldsymbol{\xi} / \partial t = \mathbf{v}$ ) and the plasma density. Outside the plasma the vacuum field is perturbed and produces a pressure on that region. In order to matching the magnetic pressure inside and outside of the plasma, a small compressive component must be added to the plasma displacement, the magnitude of which will be determined by matching the pressure at the boundary between the plasma and the vacuum. Also, the absence of any field in the region between plasma and vacuum should be considered. Finally, the momentum equation is as follows:

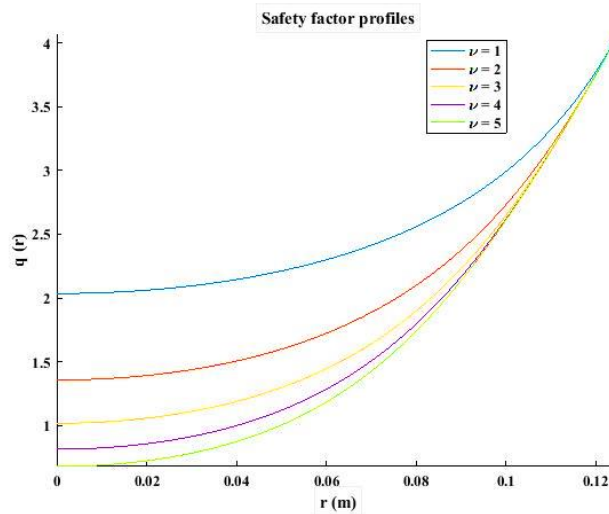
$$\rho_0 \frac{\partial^2 \xi_0}{\partial t^2} = \mathbf{F}(\xi) = \frac{2B_0^2}{\mu_0 q R_0^2} \left( \frac{b^2-1}{a^2-q} \right) \left( \frac{1}{q} - 1 \right) \xi_0 \quad (7)$$

where  $\xi = \xi_0$  is considered. When  $1 > q > \left(\frac{a^2}{b^2}\right)$ , we will have an internal kink instability with the following growth rate [14]:

$$\gamma = \sqrt{\frac{2B_0^2}{\mu_0 \rho_0 q R_0^2} \left( \frac{b^2-1}{a^2-q} \right) \left( \frac{1}{q} - 1 \right)} \quad (8)$$

Now, by providing characteristic data of IR-T1 tokamak in Table 1, the safety factor profiles and growth rate will be calculated.

Table 1. Characteristic data of IR-T1 tokamak [13].



Parameters	IR-T1 Tokamak
$R$	45 cm
$a$	12.5 cm
$b$	15 cm
$B_\phi$	0.75 T
$\rho_0$	$1.1 \times 10^{19} \text{ m}^{-3}$
$I_p$	$\sim 32.5 \text{ kA}$

### 3 Simulations and Results

In this section, we present growth rate and safety factor profiles, equations (4) and (8), in Figs. 1 and 2, to evaluate the stability of this mode in the IR-T1 tokamak. This is done entirely through programming in MATLAB software and its tools.

### safety factor in IR-T1

In Fig. 1, with  $\nu$  value of  $q$  Because  $q > 1$  is condition for the internal kink 1,2,3 the plasma against this mode

$\nu = 4$  and  $\nu = 5$  in some areas, especially in the more central areas of the plasma,  $q < 1$  and the stability, albeit locally, will be lost which can be linked to the sawtooth instability and cause plasma loss. It can be seen that at the plasma boundary ( $r = a$ ), all values of  $q$  tend to the same value ( $q(a) \sim 3.9$ ) while at the center of the plasma they have different values (from 0.68 to 2.06). Using the safety factor profile obtained in Fig. 1, the desired growth rate for IR-T1 tokamak was calculated through equation (8) and the results are presented in Fig. 2. As can be seen, for  $\nu = 1, 2, 3$  the real part (indicating instability) has no value in all areas and shows no instability. The imaginary part (indicating stability) is almost constant for  $\nu = 1$  and has the highest value but for  $\nu = 2$  and  $\nu = 3$ , it is changing so that it has the lowest value in the center and the highest value near the plasma boundary. For  $\nu = 4, 5$  the real part has the highest value in the central areas, which indicates the growth of instability. Reflecting on the results, for all  $\nu$  values, we see the highest mode stability near the IR-T1 plasma boundary. Another point is the instability overlap of values  $\nu = 4$  and 5 in a specific part of the central plasma region, which allows instability to occur in that part for both values. Finally, it can be seen that for all values,  $q(a) \sim 4$  and this value has already been confirmed in reference [15].

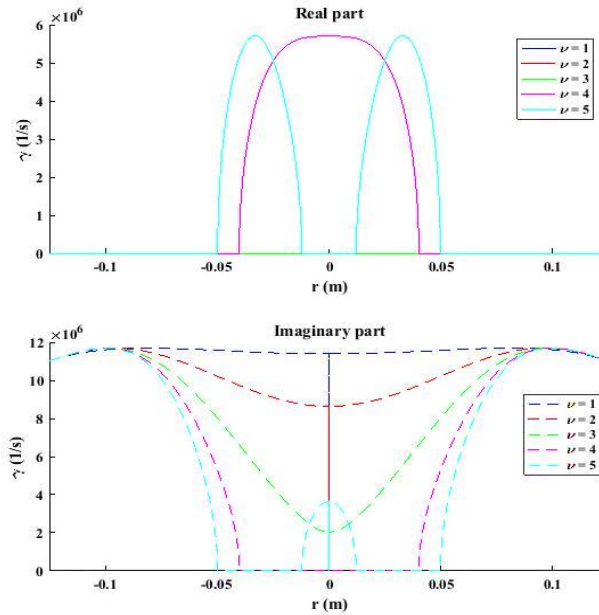


Figure 1. The profile by eq. (4) tokamak.

increasing the decreases. the minimum stability of the mode, then for  $\nu =$  will be stable in all regions. For

Figure 2. The growth rate of internal kink instability (Real part of eq. (8)) and Imaginary, or stable, part of eq. (8) for this mode in IR-T1 tokamak for values  $\nu = 1,2,3,4,5$ .

The internal kink mode is a pure toroidal mode, so it will be possible to study the growth rate of this pressure gradients-driven mode by analyzing the poloidal beta profile. This is done using one of the most up-to-date related codes, KINX. One of the obtained relationships for the growth rate of internal kink instability, which is approved and used in a wide range of plasma parameters in different tokamaks, has been obtained by fitting experimental data with KINX analytical code as follows [16]:

$$\gamma\tau_A = 0/44 \frac{\epsilon_1\kappa_1}{1+7\epsilon_1s_1} (\beta_{p1} - \beta_p^c) \quad (9)$$

$$\beta_p^c = 0.9 - (0.6 + 0.1 s(r))\kappa_1 \quad (10)$$

$$s(r) = \frac{r}{q(r)} \frac{dq(r)}{dr} \quad (11)$$

In these relations, index 1 is used to specify the desired parameter at the level corresponding to  $q = 1$ . Also  $\kappa$ ,  $s$ ,  $\epsilon$  and  $\tau_A$ , respectively, represent the plasma elongation, magnetic shear, inverse aspect ratio and Alfvénic time  $\tau_A = \sqrt{3} \frac{R_0}{v_A}$  (which  $v_A$  is Alfvénic velocity). High values of magnetic shear guarantee stability because they reduce the radial expansion of spiral resonance modes. Negative values of magnetic field, due to instabilities driven by the curvature of the magnetic field, can also cause stability. It also introduces a critical value for the poloidal beta (at which the growth rate becomes zero) at the level corresponding to  $q = 1$ . It is important to note that in this approach the total plasma current, the surface radius corresponding to  $q = 1$ , the pressure profile and the parallel current profile relative to the small plasma radius are kept constant in different states [17]. Given that the growth rate of the internal kink instability is non-zero for the values of  $\nu = 4$  and 5 and that in the approach leading to the above relations  $\Delta q = 1 - q(0) \ll 1$ , we focus our calculations in this section to these two values. The values required in the above equations for IR-T1 tokamak are as follows in Table 2 [15]. In first step the magnetic shear profile (equation (11)), using the safety factor profile, is shown in Fig. 3. From this figure,  $s_1$  values can be obtained in IR-T1 tokamak equal to  $0.042 \times 10^{-6}$  in the case of  $\nu = 4$  and equal to  $-0.323 \times 10^{-6}$  in the case of  $\nu = 5$ .

Table 2. The required values in fitting calculations with KINX code for IR-T1 tokamak.

Parameters for $\nu = 4 - 5$	IR-T1 tokamak
$r_1$	5- 4 cm
$\kappa_1$	1-1

$\epsilon_1$	0.32- 0.417
$q(0)$	0.75- 0.5
$\beta_{p1}$	0.98- 0.99

Figure 3. Magnetic values  $\nu = 4,5$  in

By specifying the profile as well as the be obtained for this 4 and 5, which is The  $\gamma\tau_A$  values are equal to 0.09574

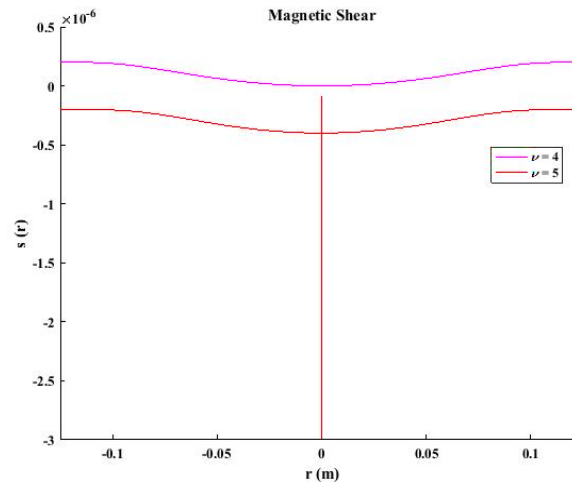
0.1266 for  $\nu = 5$ . The amount of Alfvénic time for this tokamak is:

$$\tau_A = \sqrt{3} \frac{R_0}{v_A} = \sqrt{3} \frac{R_0 \sqrt{\mu_0 \rho_e m_i}}{B} = 0.158 \mu s$$

Therefore, the  $\gamma$  values for  $\nu = 4$  and 5 are  $0.6 \times 10^6 s^{-1}$  and  $0.8 \times 10^6 s^{-1}$ , respectively. The comparison of this approximate value with the maximum growth rate in Fig. 2 is a relative confirmation, at least in terms of the order of the values, on our calculations.

#### 4 Conclusions

The ideal MHD instabilities due to the current or pressure gradient represent the final boundary of the operating limits for most magnetic fusion configurations. These possible instabilities fall into the category of ideal and resistance states. The ideal internal kink instability has been considered as an effective factor in disruptions and therefore in this work the stability of this mode in IR-T1 tokamak has been investigated. In this study, we found that instability associated with internal kink only grew locally for higher  $\nu$  values (4,5) and in the central regions of the plasma. Therefore, this instability can be prevented by adjusting the toroidal current density profile. Also, for all quantities,



shear profile for IR-T1 tokamak.

magnetic shear  $s_1$  values,  $\gamma\tau_A$  can tokamak for  $\nu =$  shown in Fig. 4. obtained in Fig. 4 for  $\nu = 4$  and

we saw the most stability for this mode near the plasma boundary. A typical comparison with the results of fitting the data with the KINX simulation code also shows a good agreement in terms of the order of the obtained values. Finally, the study of time variation of safety factor and consequently the growth rate of internal kink instability, detailed study of poloidal magnetic flux functions and considering nonlinear effects as well as resistance effects on the growth rate of internal kink instability can have different and remarkable results for the performance of tokamak during its discharge compared to the linear results obtained in this study, which will be the subject of future works.

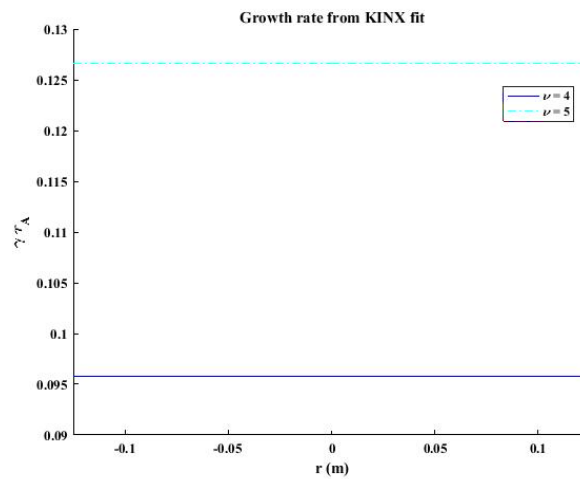


Figure 4. The kink instability code results in IR-

growth rate of internal from fitting of KINX T1 tokamak for values

$$\nu = 4,5.$$

## References

- [1] S. Ortolani and D.D. Schnack, 1993. Magnetohydrodynamics of Plasma Relaxation, World Scientific Publishing, Singapore Pte Ltd, pp. 15-43.
- [2] R.J. Hosking, "Computation of Visco-resistive MHD Instabilities", Journal of Comput. Physics. 66, 274 (1986).
- [3] A. Gsponer, 2009. "Physics of high-intensity high-energy particle beam propagation in open air and outer-space plasmas", arXiv: Plasma Physics. /0409157v 3.
- [4] H. Zohm, 2015. Magnetohydrodynamic Stability of tokamaks, 1st ed., Wiley-VCH, Garching.
- [5] Ph.D thesis, V.S. Lukin, 2008. "Computational study of the internal kink mode evolution and associated magnetic reconnection phenomena". Princeton University, MA. Retrieved from <https://ui.adsabs.harvard.edu/abs/2008PhDT.....1>.
- [6] Ph.D thesis, L H. de Blank, 1990. "Theory of the m=1 kink mode in toroidal plasmas". The National University in Utrecht. Retrieved from [https://inis.iaea.org/collection/NCLCollectionStore/\\_Public/22/006/22006377.pdf](https://inis.iaea.org/collection/NCLCollectionStore/_Public/22/006/22006377.pdf)
- [7] J. Mendonca, et al., 2019. "Simulation of the internal kink mode in visco-resistive regimes", arXiv: Physics.plasma-ph, 1911.04028v1.
- [8] C. Angioni, et al., "Effects of localized electron heating and current drive on the sawtooth period", Nucl. Fusion. 43, 455 (2003).
- [9] Ph.D thesis, L. Guazzatto, 2005. "Equilibrium and stability of tokamak plasmas with arbitrary flow". University of Rochester, Rochester, New York. Retrieved <https://www.lle.rochester.edu/media/publications/documents/theses/Guazzotto.pdf>
- [10] T. Kass, et al., "The fishbone instability in ASDEX Upgrade", Nucl. Fusion, 38, 807 (1998).
- [11] S. Günter, et al., "Influence of fishbones on the background plasma", Nucl. Fusion, 39, 1535 (1999).



- [12] F. Dini and S. Khorasani, “Study of magnetohydrodynamic stability in Damavand tokamak with large aspect ratio”, J. of Nuclear Sci. and Tech, 49, 14 (2009) (In Persian).
- [13] M. Ghoranneviss, et al., “Measurements of the plasma current density and Q-profiles in IR-T1 tokamak”, Journal of Fusion Energy. 29(3), 232 (2010).
- [14] S. Cowley, 2007. Introduction to kink modes-the Kruskal-Shafranov limit, UCLA, Lecture# 3; J.P. Friedberg, 1987. Ideal magnetohydrodynamics, 1st ed., Plenum, New York.
- [15] M. Ghoranneviss and S. Meshkani, 2017. *Plasma Science and Technology for Emerging Economies*, edited by R.S. Rawat, Springer Nature, Singapore Pte Ltd, pp. 413-474.
- [16] L. Degtyarev, et al. “The KINX ideal MHD stability code for axisymmetric plasmas with separatrix”, Comput. Phys. Commun. 103(1), 10 (1997).
- [17] A. Martynov, J.P. Graves and O. Sauter, “The stability of the ideal internal kink mode in realistic tokamak geometry”, Plasma Phys. Control. Fusion 47, 1743 (2005).

## Hawking Radiation for Hayward Black hole in Einstein–Gauss–Bonnet Gravity through Tunneling Process

Shadi Shahraeini<sup>1</sup>, Kouros Nozari<sup>2</sup>, Sara Saghafi<sup>3</sup>

<sup>1</sup>Department of Theoretical Physics, University of Mazandaran, Babolsar.

Email: s.shahraeini02@umail.umz.ac.ir

<sup>2</sup>Department of Theoretical Physics, University of Mazandaran, Babolsar.

Email: knozari@umz.ac.ir

<sup>3</sup>Department of Theoretical Physics, University of Mazandaran, Babolsar.

Email: s.saghafi@umz.ac.ir

**Abstract.** The Einstein-Gauss-Bonnet theory (EGB) can be considered as one of the most promising candidates for modified gravity. In this paper we intend to obtain the Hawking radiation of a 5-dimensional Hayward black hole with a regular center, having inner (Cauchy) and outer (event) horizons in EGB theory. We present a short derivation of Hawking radiation as a tunneling process, based on particles in a dynamical geometry. The imaginary part of the action for the classically forbidden process is related to the Boltzmann factor for emission at the Hawking temperature.

Keywords: Hawking radiation, Hayward Black holes, Einstein-Gauss-Bonnet Theory

### 1 Introduction

black holes are the exact solution of the Einstein's general relativity, appear to exist in the universe, with singularities form inside them [1]. However, the existence of a singularity means space–time ceases to exist signaling the breakdown of general relativity, requiring modifications that believably include quantum theory. One of the steps in this direction, regular (i.e.non-singular) black holes have widely considered resolving the singularity problems, dating back to Bardeen [2] who gave first regular black hole model by Bardeen [2], according to whom there are horizons but there is no singularity. Hayward [3] proposed, Bardeen-like, regular space–times are given that describe the formation of a black hole from an initial vacuum region which has a finite density and pressure, vanishing rapidly at large small and behaving as a cosmological constant at a small distance. It is a simple exact model of general relativity coupled to electrodynamics and hence Hayward black hole has attracted significant attention in various studies, like Quasinormal modes of the black holes by Lin et al. [4], The geodesic equation of a particle by Chiba and Kimura [5], wormholes from the regular black hole [6,7] with their stability [8], black hole thermodynamics [9] and related properties [10,11], and strong deflection lensing [12]. The rotating regular Hayward's metric has been studied as a particle accelerator [13,14].

In the last few decades, there has been a noteworthy number of attempts in higher dimensions gravity in order to understand the low-energy limit of string theory. The Einstein–Gauss–Bonnet gravity is a very important higher dimensional generalization of Einstein's gravity which was suggested by Lanczos [15], and then rediscovered by David Lovelock [16]. The study of Einstein–Gauss–Bonnet theory becomes very important since it provides a broader setup to explore a lot of conceptual issues related to gravity. This theory is completely free of ghost and the order of the field equations in the Einstein–Gauss–Bonnet theory is no higher than two. Since their outset, there

has been a lot of attempts to obtain the black hole solution, but Boulware and Deser were the first to obtain the exact black hole solution in the Einstein–Gauss–Bonnet gravity [17,18]. After that several exact black hole solutions with their thermodynamical properties have been discussed by various authors [19,20]. Several black hole solutions with matter source generalizing the Boulware–Desser solution have also been explored [21,22].

A natural question to ask: what is the effect of the Einstein–Gauss–Bonnet correction on the regular black holes and their properties? In order to answer this question, one would first need a regular solution for the Einstein–Gauss–Bonnet theory. In [23] they obtained a 5D spherically symmetric and static Hayward-like black hole solution of the Einstein–Gauss–Bonnet gravity. It turned out that the metric proposed there is an exact black hole model of Einstein–Gauss–Bonnet having minimal coupling with nonlinear electrodynamics thereby it is the generalization of the Boulware–Desser solution.

In this paper we aim to study the tunneling of the massless particles from the event horizon of 5D EGB-Hayward black holes and we will investigate the correlation between the emission modes and temperature of this horizon. This paper is organized as follows: In section 2, we have a short review of the structure of the 5D EGB-Hayward black holes with a regular center and two horizons. In section 3, we explain the tunneling process and illustrate the temperature of the 5D EGB-Hayward black holes. Section 4 contains a summary and conclusion.

## 2 5D exact Hayward-like black holes in EGB gravity

The general relativity with minimal coupling with nonlinear electrodynamics leads to exact spherically symmetric regular black holes [24,25,26,27]. The two most famous exact black holes are Bardeen [2] and Hayward [3] regular black holes. Here, we are interested in the Hayward-like black hole solution with a regular center in the EGB gravity in 5D space-time. we use the metric ansatz [28]:

$$ds^2 = -f(r)dt^2 + \frac{dr^2}{f(r)} + r^2 d\Omega_3^2, \quad (1)$$

Where  $d\Omega_3^2 = d\theta^2 + \sin^2\theta(d\phi^2 + \sin^2\phi d\Psi^2)$  is the metric in the 3D hypersurface with volume  $V_3$  and  $f(r)$  is the metric function:

$$f(r) = 1 + \frac{r^2}{4\alpha} \left( 1 \pm \sqrt{1 + \frac{8\alpha m}{r^4 + e^4}} \right) \quad (2)$$

Here,  $m$  is a constant of integration having the relation with the Arnowitt-Deser-Misner (ADM) mass  $M$  of the black hole with the relation of

$$M = \frac{3V_3}{k_5} m \quad (3)$$

Here,  $V_3$  is the volume of a 3-dimensional unit sphere and the metric has a coordinate singularity at the horizon. It is found that, when  $m \neq 0 \neq \alpha$ , the invariants are well behaved everywhere including at  $r = 0$ . Thus, the 5D Hayward like black holes have no singularity or they are regular. It turns out that  $g^{rr} = f(r_H) = 0$  is only coordinate singularity implies the presence of horizons. After some calculations, the location of horizon is

$$r_+^2 = \frac{1}{3} \left[ m - 2\alpha - \frac{2^{\frac{2}{3}}(3e^4 - (m - 2\alpha)^2) + \beta^2}{2^{\frac{1}{3}}\beta} \right] \quad (4)$$

with

$$\beta = 2(m - 2\alpha)^2 + 12m\alpha^2 - 18(m + 4\alpha)e^4 + \sqrt{(2(m - 2\alpha)^2 + 12m\alpha^2 - 18(m + 4\alpha)e^4)^2 + 4((3e^4 - (m - 2\alpha))^3)} \quad (5)$$

It is possible to keep the value of mass  $m$  and coupling constant  $\alpha$  fixed, then we come to find out that there exists a critical value of charge ( $e_E$ ), such that the Cauchy ( $r_-$ ) and the event horizons ( $r_+$ ) coincide, i.e.,  $r_- = r_+$ , corresponds to the extremal 5D EGB-Hayward black holes with degenerate horizon radius ( $r_E = r_{\pm}$ ). So, when  $e < e_E$ , black holes with Cauchy and event horizons exist and for any value of charge  $e > e_E$ , there exists only a regular space-time but not black holes.

### 3 Hawking Radiation of the 5D EGB-Hayward Black holes with Tunneling Process

In the intelligent approach that Parikh and Wilczek have provided two issues are considerable: energy conservation and dynamical geometry [30-32]. In this picture, particle, and antiparticle are created with zero total energy in the near of one side of the horizon, after that one particle tunnels from the horizon in a semiclassical way. A particle tunnels through a barrier created by the particle's energy itself. As a result, the radius and mass of the black hole reduce as much as the particle of energy  $\omega$ . The first step to the calculation of particle tunneling is the construction of the nonsingular line element on the horizon. To resolving horizon singularity, we use the Painlevé coordinate transformation with definition  $t_p$  by  $t_p = t - f(r)$ . Applying this transformation on the metric (1), we will have a new nonsingular coordinate as follows

$$ds^2 = -f(r)dt^2 + 2\sqrt{1 - f(r)}drdt + dr^2 + r^2d\Omega_3^2 \quad (6)$$

Now, we present the primary calculation of the temperature of the black hole with the tunneling process. A particle is moving from an initial state in  $r_{in}$  to the final state in  $r_{out}$  as  $r_{in} > r_{out}$ . Tunneling calculation based on to account the imaginary part of the action for this particle as follows

$$Im S = Im \int_{r_{in}}^{r_{out}} p_r dr = Im \int_{r_{in}}^{r_{out}} \int_0^{p_r} dp'_r dr \quad (7)$$

where  $r_{in} = r_H - \epsilon$  and  $r_{out} = r_H + \epsilon$ ,  $\tilde{\omega}$  is particles' energy which is known as a self-interaction. Putting Hamilton equation,  $dp_r = \frac{dH}{\dot{r}}$ , on the Eq. (7), we have

$$I = \int_{r_{in}}^{r_{out}} \int_M^{M-\omega} \frac{dr}{\dot{r}} dH = \int_0^\omega \int_{r_{in}}^{r_{out}} \frac{dr}{\dot{r}} (-d\tilde{\omega}) \quad (8)$$

Because we note the massless particles' tunneling, we determine the light-like geodesics regarded to transformed metric (Eq. (6)) as follows

$$\dot{r} = \pm 1 - \sqrt{1 - f(r)} \quad (9)$$

where + and - signs indicate the outgoing and ingoing geodesics, respectively. With considering outgoing trajectories and substituting Eq. (9) in Eq. (8), we find the imaginary part of the action as follow

$$Im S = -Im \int_0^\omega \int_{r_{in}}^{r_{out}} \frac{dr d\tilde{\omega}}{1 - \sqrt{1 - f(r)}} \quad (10)$$

In the tunneling process, since it is a near horizon phenomenon, particles created near the inside of black hole horizon are located at  $r_{in} = r_+$ , then these tunnel from black hole horizon and reach

the outside of it which is located at  $r_{out} = \frac{1}{3} [(m - \omega) - 2\alpha - \frac{2^{\frac{2}{3}}(3e^4 - ((m - \omega) - 2\alpha)^2) + \beta^2}{2^{\frac{1}{3}}\beta}]^{\frac{1}{2}}$ , where  $\omega$

is the particle's shell of energy. To calculate the imaginary part of the action, we replace Eq. (2) in Eq. (10), as follows

$$ImS = -Im \int_0^\omega \int_{r_{in}}^{r_{out}} \frac{dr d\tilde{\omega}}{1 - \sqrt{\frac{r^2}{4\alpha} (1 \pm \sqrt{1 + \frac{8\alpha m}{r^4 + e^4}})}} \quad (11)$$

This integral has two poles, so, to deduce the poles we expand the denominator in terms of  $r_{out}$  as follows

$$\dot{r} = 1 - \sqrt{1 - [f(r_{out}) + f'(r_{out})(r - r_{out}) - \dots]} \quad (12)$$

where a prime indicates derivative with respect to  $r$ . we compute the first integral with residue calculus and expand the result to the second order of  $\omega$ . Calculating the second integral, we derive the imaginary part of the action in terms of particles' energy and the black hole mass. According to the relation between the emission rate, the imaginary part of the action, and the Boltzmann factor

$$\Gamma \simeq e^{-2ImS} = e^{-\beta\omega} \quad (13)$$

the temperature of the black hole can be calculated since the Hawking temperature is the inverse of the Boltzmann factor,  $T = \frac{1}{\beta}$ . Finally, we derive the temperature of the black hole horizon in terms of the black hole mass and the coupling constant. We plot the temperature of the black hole horizon of the 5D exact Hayward-like black holes in EGB gravity as a function of the mass of the black hole in Fig. (1) with  $\alpha = 0.1, 0.2, 0.4, 0.6$ . By reducing the mass of the black hole, the temperature increases to a maximum temperature when the black hole mass reaches a special mass. After, reducing mass, the temperature reduces, too. On the other hand, by reducing the coupling constant, maximum temperature of the black hole horizon increases. For comparison, we plotted the standard hawking temperature. It is clear that in the final stage of evaporation the standard Hawking temperature goes to infinity and is divergent but for this 5D EGB-Hayward black hole, the presence of coupling constant leads to have a zero temperature at the final stage of evaporation.

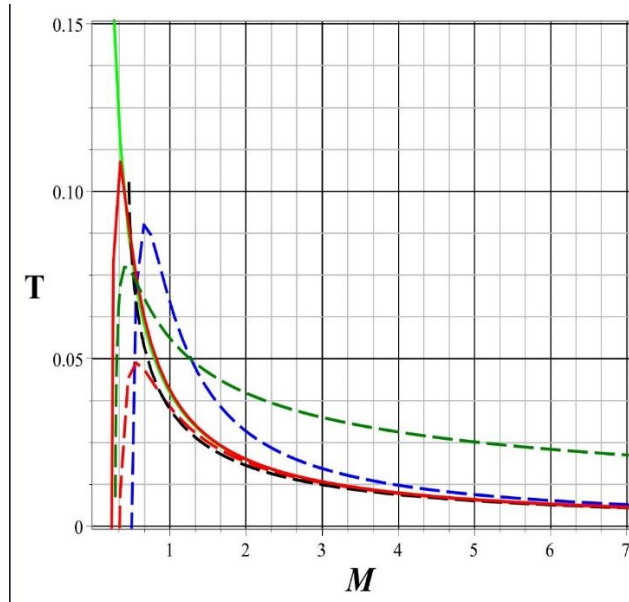


Fig (1): Temperature of the 5D exact Hayward-like black holes in EGB gravity versus Mass. The figure has been plotted with  $\alpha = 0.1, 0.2, 0.4, 0.6$  from up to down. The green plot is for standard Hawking temperature for Schwarzschild black hole

## 4 Conclusions

In this work, we investigated the 5D exact Hayward-like black hole in EGB gravity and their radiation and temperature. We calculated the tunneling of the massless particles from the event horizon of 5D EGB-Hayward black hole and we investigated the temperature of this horizon. The temperature of the black hole horizon of the 5D exact Hayward-like black hole in EGB gravity was plotted as a function of the mass of the black hole in Fig. (1) with  $\alpha = 0.1, 0.2, 0.4, 0.6$ . By reducing the mass of the black hole, the temperature increases to a maximum temperature when the black hole mass reaches a special mass. After, reducing mass, the temperature reduces, too. On the other hand, by reducing the coupling constant, maximum temperature of the black hole horizon increases. We concluded that in the final stage of evaporation the standard Hawking temperature goes to infinity and is divergent but for this 5D EGB-Hayward black hole, the presence of coupling constant leads to have a zero temperature at the final stage of evaporation.

## References

- [1] S. W. Hawking and G. F. R. Ellis, *The Large Scale Structure of Spacetime* (Cambridge University Press, Cambridge, 1973).
- [2] J. Bardeen, in *Proceedings of GR5, Non-singular general-relativistic gravitational collapse* (Tiflis, U.S.S.R., 1968).
- [3] S. A. Hayward, *Formation and Evaporation of Nonsingular Black Holes* *Phys. Rev. Lett.* 96, 031103 (2006).
- [4] K. Lin, J. Li and S. Yang, *Quasinormal modes of gravitational field perturbation of regular phantom black holes*, *Int. J. Theor. Phys.* 52, 3771 (2013).
- [5] T. Chiba and M. Kimura, *A note on geodesics in the Hayward metric*, *PTEP* 2017, no. 4, 043E01 (2017).
- [6] M. Halilsoy, A. Ovgun and S. H. Mazharimousavi, *Thin-shell wormholes from the regular Hayward black hole*, *Eur. Phys. J. C* 74, 2796 (2014).
- [7] P. K. F. Kuhfittig, Aditi J. Math, *Hayward black holes in the novel 4D Einstein-Gauss-Bonnet gravity*, *Phys.* 5, 25 (2014).
- [8] M. Sharif and S. Mumtaz, *Stability of the Regular Hayward Thin-Shell Wormholes*, *Adv. High Energy Phys.* 2016, 2868750 (2016).
- [9] R. V. Maluf and Juliano C.S, *Thermodynamics of a class of regular black holes with a generalized uncertainty principle*, *Neves Phys. Rev. D* 97, 104015 (2018).
- [10] A. Abdujabbarov, M. Amir, B. Ahmedov and S. G. Ghosh, *Shadow of rotating regular black holes*, *Phys. Rev. D* 93, 104004 (2016).
- [11] S. H. Mehdipour and M. H. Ahmadi, *Black Hole Remnants in Hayward Solutions and Noncommutative Effects*, *Nucl. Phys. B* 926, 49 (2018).
- [12] S. S. Zhao and Y. Xie, *Strong deflection gravitational lensing by a modified Hayward black hole*, *Eur. Phys. J. C* 77, 272 (2017).
- [13] B. Gwak, *Collision of two rotating Hayward black holes*, *Eur. Phys. J. C* 77, 482 (2017).
- [14] M. Amir and S. G. Ghosh, *Horizon structure of rotating Bardeen black hole and particle acceleration*, *JHEP* 1507, 015 (2015).

- [15] C. Lanczos, A Remarkable Property of the Riemann-Christoffel Tensor in Four Dimensions, *Ann. Math.* 39, 842 (1938).
- [16] D. Lovelock, The Einstein Tensor and Its Generalizations, *J. Math. Phys. (N.Y.)* 12, 498 (1971).
- [17] D. G. Boulware and S. Deser, String-Generated Gravity Models, *Phys. Rev. Lett.* 55, 2656 (1985).
- [18] R. C. Myers and J.Z. Simon, Black-hole thermodynamics in Lovelock gravity, *Phys. Rev. D* 38, 2434 (1988).
- [19] Y. M. Cho and I.P. Neupane, Anti-de Sitter Black Holes, Thermal Phase Transition and Holography in Higher Curvature Gravity, *Phys. Rev. D* 66, 024044 (2002).
- [20] C. Sahabandu, P. Suranyi, C. Vaz and L.C.R. Wijewardhana, Thermodynamics of static black objects in D dimensional Einstein-Gauss-Bonnet gravity with D-4 compact dimensions, *Phys. Rev. D* 73, 044009 (2006).
- [21] S. H. Mazharimousavi and M. Halilsoy, Lovelock black holes with a power-Yang-Mills source, *Phys. Lett. B* 681, 190 (2009).
- [22] S. G. Ghosh and S. D. Maharaj, Cloud of strings for radiating black holes in Lovelock gravity, *Phys. Rev. D*, 89, 084027 (2014).
- [23] A. Kumar, D. Singh and S. Ghosh, Hayward black holes in Einstein-Gauss-Bonnet gravity, *Annals of Physics* 419 (2020) 168214
- [24] I.G. Dymnikova, DE SITTER-SCHWARZSCHILD BLACK HOLE: ITS PARTICLELIKE CORE AND THERMODYNAMICAL PROPERTIES, *Int. Journal of Mod. Phys. D*, 5 529 (1996).
- [25] I. G. Dymnikova, Micha Korpusik, Regular Black Hole Remnants, *Phys. Lett. B* 685, 1218 (2010).
- [26] E. Ayon-Beato and A. Garcia, Non-Singular Charged Black Hole Solution for Non-Linear Source, *Gen. Rel. Grav.* 31, 629 (1999).
- [27] E. Ayon-Beato, A. Garcia, The Bardeen Model as a Nonlinear Magnetic Monopole, *Phys. Lett. B* 493, 149 (2000).
- [28] S. G. Ghosh and S. D. Maharaj, Radiating Kerr-like regular black hole, *Eur. Phys. J. C* 75, 7 (2015).
- [29] I. Perez-Roman and N. Brent, *Gen. Rel. Grav.* 50, no. 6, 64 (2018).
- [30] M. K. Parikh and F. Wilczek, Hawking Radiation as Tunneling, *Phys. Rev. Lett.* 85, 5042 (2000), [hep-th/9907001].
- [31] M. K. Parikh, A Secret Tunnel Through the Horizon, *Int. J. Mod. Phys. D* 13, 2351 (2004), [hep-th/0405160]; M. K. Parikh, Energy Conservation and Hawking Radiation, (2004) [arXiv: hep-th/0402166].
- [32] P. Kraus, F. Wilczek, Self-Interaction Correction to Black Hole Radiance, *Nucl. Phys. B* 433, 403 (1995), [gr-qc/9408003].

## Modified AdS/QCD model in an external electric field

Leila Shahkarami

School of Physics, University of Damghan, Damghan, 41167-36716

Email: l.shahkarami@du.ac.ir

**Abstract.** We consider the response of a holographic magnetized bottom-up theory to an external electric field. Our main purpose here is to study the effect of modifying the scale factor on the pair production in the presence of the background magnetic field. According to [3] this modification was used to remove the sudden flattening in the quark-antiquark potential in order to have a confining theory for any given values of  $B$ . We see that changing the scale factor to the new modified one, which is magnetic-field-dependent, decreases the chance of the pair production, since it enhances both the critical electric fields and the height and width of the total potential. Moreover, by increasing the magnetic field perpendicular to the separation direction of the quarks, the production of the quarks becomes harder with the new scale factor unlike the quadratic scale factor. In the theory with the quadratic scale factor almost always the magnetic field facilitates the production of the quarks from the vacuum.

Keywords: AdS/QCD, Confinement-deconfinement phase transition, Electromagnetic field

### 1 Introduction

Investigating the response of QCD to electric and magnetic fields is a very important problem, both theoretically and experimentally. From the theoretical point of view, particle pair production from the vacuum due to the presence of an electric field [1] could reveal many unknown features of the quantum vacuum regarding the non-perturbative nature of the phenomenon. On the other hand, there are important realistic situations that our system is subjected to electromagnetic fields, e.g., a strong magnetic field along with an electric field is created at early times after heavy ion collisions in RHIC and LHC experiments.

Due to the non-perturbative nature of such phenomena and the strong coupling in the system, the use of the AdS/CFT correspondence [2] and in general holography could be very fruitful. Employing these methods by the vast amount of works done in the context of Holographic Schwinger effect have led us to interesting results. For instance, these studies show that there are two critical electric fields for each holographic theory;  $E_s$  is the electric field below which no charged pair particles can be produced from the vacuum and  $E_c$  is the electric field above which the Schwinger effect occurs catastrophically. Between these two values the pairs are freed through a tunneling process.

Most of these studies consider the problem when only the electric field is present using the top-down models or phenomenological bottom-up models which are not the solution to the gravity equations. Here we employ a magnetized bottom-up model which is a solution to the equations of motion and can mimic the behavior of QCD, well. As in [3] we choose two different warp factors and compare the response of the resulting theory to a fixed external electric field for the two warp factors. The chosen theory is equipped with a background fixed magnetic field. Thus, we are able to study the effect of the external electric field on a confined QCD-like theory with a background magnetic field, which is a less-studied problem and hence worth considering.

## 2 The gravitational background

In this section we introduce the bulk theory used for our study. The 5-dimensional metric of the gravity side is as follows:

$$ds^2 = L^2 S(r) \left[ -r^2 dt^2 + \frac{dr^2}{r^2} + r^2 dx^2 + r^2 e^{\frac{B^2}{r^2}} dy^2 \right], \quad (1)$$

where  $L$  is the AdS radius,  $B$  is the magnetic field applied in the  $x$  direction and  $r$  is the AdS radial position which goes to infinity at the boundary. This is the solution found in [4] for the equations of the Einstein-Maxwell-dilaton (EMD) model with two Maxwell fields and one scalar field with a potential term. The form factor in the string frame is in the form  $S(r) = e^{2\left(A(r) + \frac{\phi(r)}{\sqrt{6}}\right)}$  in which  $\phi(r)$  is the scalar field and  $A(r)$  can be chosen at will. Here, we work with the form  $A(r) = -\frac{b}{r^2} - d \frac{B^2}{r^5}$  as in [3], where  $d = 0$  corresponds to the first form chosen there which gives the model studied in [4]. In the present study we focus on the case with no black hole, which is expected to explain the confining phase of the field theory side. To that purpose, we have set the blackening function equal to one in the ansatz metric (1).

As they have illustrated, the choice of  $d = 0$  raises a problem in the confining phase of the system. When one calculates the separating length of a quark and an antiquark in the same direction as the magnetic field, its linear behavior (a sign for the confinement) disappears at a finite separation, meaning that the profile of two straight open strings is preferred to a U-shape open string. To avoid this problem, they considered a new scale factor with  $d$  in [3] and showed that this scale factor guarantees that for every value of the magnetic field the confinement is seen and also the theory would be physically reliable for higher values of  $B$ . We should mention that for both scale factors high enough value of  $B$  leads to the imaginary values for the scalar field. This critical  $B_{crit}$  is about 0.61 for  $d = 0$  and is higher for  $d$  depending on the exact value of  $d$ . At  $d = 0.013$  we have  $B_{crit} = 1.025$ . This value of  $d$  is the highest value that leads to the inverse magnetic catalysis which is compatible with the result of the lattice calculations. Notice that in our calculations we set  $b = 0.15$ , the value obtained through comparison with the results found by the lattice calculations at zero magnetic field. All the quantities are in unit  $GeV$ . We will work with  $d = 0.013$  throughout this paper.

In the next section we investigate the response of the system of our interest to a fixed external electric field by analyzing the total potential of a quark-antiquark pair placing in fixed positions in the field theory side.

## 3 Response to the electric field

Consider a quark and an antiquark of the same finite mass placing in fixed positions in the field theory side and with spatial separation  $l$  from each other. Regarding the anisotropy induced by the magnetic field, the pair of quarks could be placed along two physically different directions; in the same direction as the magnetic field and perpendicular to the magnetic field, which we denote as the longitudinal (l) and transverse (t) directions, respectively. The total potential of this pair in an external electric field  $E$  applied at the same direction as the separating direction of the quarks, is the sum of the potential of the quark-antiquark pair (calculated from the rectangular Wilson loop)

and the potential due to the interaction with  $E$ . According to the AdS/CFT dictionary, to calculate the first part, we should minimize the Nambu-Goto action of an open string hanging in the dual gravity theory. To explain the finite mass of the quarks, we attach the ends of the string to a D3-brane placed at an intermediate position  $r_0$  in the bulk. Performing these calculations, the separation length and total potential of the quarks are determined as follows:

$$l = \frac{2}{r_0 a} \int_1^{1/a} dy \frac{s(\frac{1}{r_0 a}) \sqrt{g(\frac{1}{r_0 a})}}{y^2 \sqrt{g(\frac{1}{r_0 a y})} \sqrt{y^4 s(\frac{1}{r_0 a y}) g(\frac{1}{r_0 a y}) - s(\frac{1}{r_0 a}) g(\frac{1}{r_0 a})}}, \quad (2)$$

$$V = 2 T_f L^2 r_0 a \int_1^{1/a} dy \frac{y^2 s(\frac{1}{r_0 a y}) \sqrt{g(\frac{1}{r_0 a y})}}{y^2 \sqrt{g(\frac{1}{r_0 a y})} \sqrt{y^4 s(\frac{1}{r_0 a y}) g(\frac{1}{r_0 a y}) - s(\frac{1}{r_0 a}) g(\frac{1}{r_0 a})}} - E l, \quad (3)$$

where,  $r_0$  denotes the position of the D3-brane,  $a = \frac{r_c}{r_0}$  and  $y = \frac{r}{r_c}$ .  $r_c$  is the position of the turning point of the string in the bulk. Moreover,  $g(r) = 1(e^{\frac{B^2}{r^2}})$  for the longitudinal (transverse) case.

Previous holographic studies on the effect of the electric field on the field theory vacuum, show that there exist two values of the electric field at which the physics behaves critically.  $E_s$  which is only present in the confined phase, The potential energy from the electric field is not enough to compensate the energy from the confining force. Therefore, the quarks could not be liberated. However, when we increase the electric field above  $E_s$ , the pairs can be produced through a tunneling process until we reach the second critical electric field called  $E_c$ . Above  $E_c$  the pair production occurs freely and without any obstacles. The values of these critical fields could be found from their definitions explained above, using the total potential in Eq. (3). We can also find  $E_c$  using the DBI action of the D3-brane at  $r_0$ . To follow this calculation we refer you to [5]. We can also find the formulae of the critical electric fields using the general formulae found in [6]. After doing such calculations,  $E_s$  and  $E_c$  for our system read

$$E_s = T_f \frac{S(z_w)L^2}{z_w^2} \sqrt{g(z_w)}, \quad E_c = T_f \frac{S(z_0)L^2}{z_0^2} \sqrt{g(z_0)}, \quad (4)$$

Notice that  $z_w = \frac{1}{r_w}$  shows the position of the IR wall.

## 4 Results and Discussion

Now we report the results through some graphs. First we depict the critical electric fields in the left and right graphs of Fig. 1 as functions of  $B$ , for the longitudinal and transverse cases, respectively. Solid lines show  $E_c$  and dashed lines show  $E_s$ . As can be seen, in all cases generally the magnetic field reduces  $E_c$  and  $E_s$ . It means that the magnetic field simplifies the production of the quarks. In the longitudinal case at  $d = 0$ ,  $E_s$  goes to zero suddenly at  $B = 0.36118$ , like a first order phase transition. Removing  $E_s$  means that for  $B > 0.36118$  the system under study is in the deconfinement phase. However, improving the scale factor to the one with nonzero  $B$  removes such a phase transition at a finite  $B$  such that the theory is in the confining phase regardless of the magnetic field value. This behavior is expected from Fig. 2 which shows the position of the IR

wall in the bulk. From Fig. 1 we simply see that at a given value of the magnetic field the both critical electric fields have higher values in the modified scale factor with respect to the quadratic scale factor. This means that in the presence of the magnetic field the Schwinger effect happens harder in the theory with the modified scale factor.

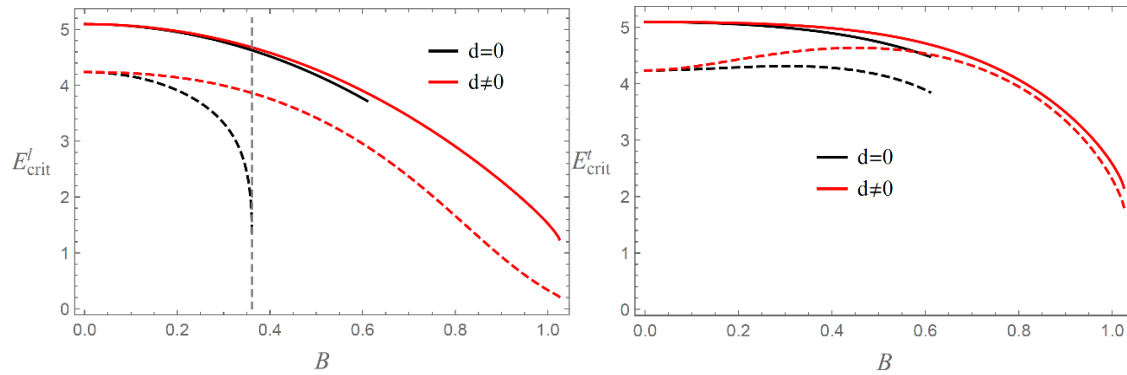


Figure 1. The critical electric fields versus  $B$  for the longitudinal and transverse cases. In both graphs, solid and dashed lines refer to  $E_C$  and  $E_S$ , respectively.

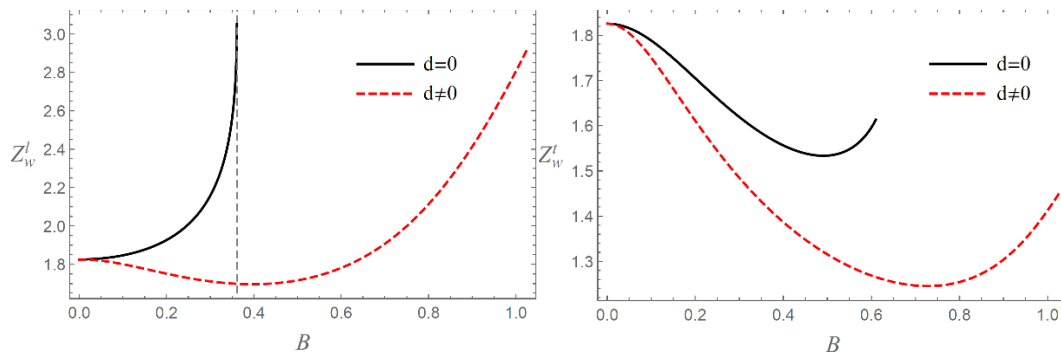


Figure 2. The position of the IR wall versus  $B$  for the longitudinal and transverse cases.

Figure 3 depicts the total potential as a function of the separation between the quarks for longitudinal and transverse cases, at a given value of the external electric field. As can be seen, both cases the quarks are facing with a bigger potential barrier in the theory with the modified scale factor. We can also infer from the right figure that the width and height of the potential barrier in the theory with the modified scale factor are larger than the case without the magnetic field. It means that in this theory the magnetic field works against the Schwinger effect in the transverse case.

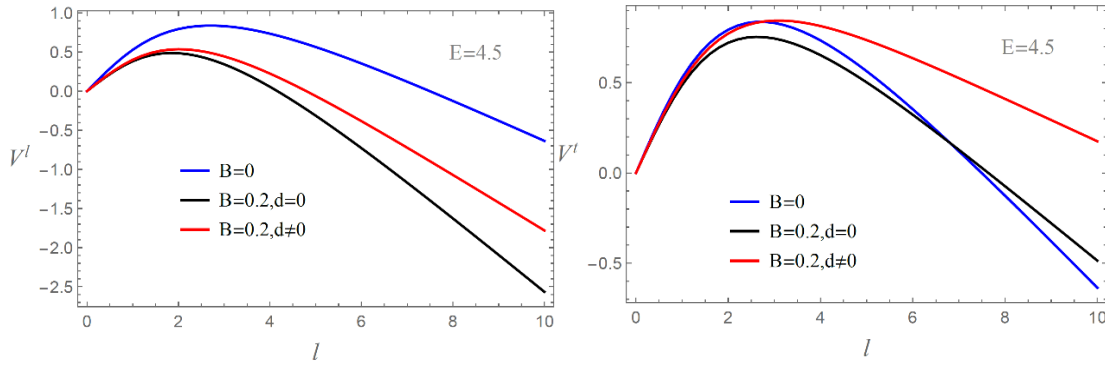


Figure 3. The total potential as a function of the separation length of the quark pair.

## 11 Conclusions

In this paper we have studied the response of a holographic magnetized EMD model to an external electric field. In this study we have focused our attention on the effect of different choices for the scale factor of the gravity metric and followed the question that how improving the warp factor and cancelling the problem of sudden change of the preferred string profile can affect the Schwinger effect. Our results have shown that the general effect of the magnetic field on the production of the quarks in the longitudinal case is not altered by improving the scale factor and as before the magnetic field simplifies the production of the quarks separated in the same direction as the magnetic field. Also, the phase transition seen in the longitudinal case at a value of  $B$  is removed when modifying the scale factor. For the same set of parameters, we have also seen that the critical electric fields are higher for the refined scale factor. We have also observed that the production of quark pairs becomes harder by increasing the magnetic field in the theory with modified scale factor unlike the model with the simple quadratic scale factor, where the magnetic field almost always favors the Schwinger effect.

## References

- [1] J. S. Schwinger, “On gauge invariance and vacuum polarization,” *Phys. Rev.* 82, 664 (1951).
- [2] J. M. Maldacena, “The large  $N$  limit of superconformal field theories and gravity,” *Adv. Theor. Math. Phys.* 2, 231 (1998); *Int. J. Theor. Phys.* 38, 1113 (1999).
- [3] H. Bohra, D. Dudal, A. Hajilou and S. Mahapatra, “Chiral transition in the probe approximation from an Einstein-Maxwell-dilaton gravity model,” *Phys. Rev. D* 103, 086021 (2021).
- [4] H. Bohra, D. Dudal, A. Hajilou and S. Mahapatra, “Anisotropic string tensions and inversely magnetic catalyzed deconfinement from a dynamical AdS/QCD model,” *Phys. Lett. B* 801, 135184 (2020).
- [5] L. Shahkarami, “Magnetized Einstein-Maxwell-dilaton model under an external electric field,” *Eur. Phys. J. C* 82, 33 (2022).
- [6] Y. Sato and K. Yoshida, “Universal aspects of holographic Schwinger effect in general backgrounds,” *JHEP* 12, 051 (2013).

## Quantum Correction to the Black Holes Thermodynamics

Behnam Pourhassan  
School of physics, Damghan University, Damghan, Iran.  
Email: b.pourhassan@du.ac.ir

**Abstract.** In this paper, we consider non-perturbative quantum correction which appears as exponential term in the black hole entropy. We study consequence thermodynamics of the Horava-Lifshitz black hole at quantum scales.

Keywords: Black hole, Thermodynamics.

### 1 Introduction

One of the finest ways to learn about black holes is to study their thermodynamics. By utilizing the surface information, the holographic principle allows us to obtain insight into black hole physics. The black hole entropy is proportional to the event horizon area and the black hole temperature is proportional to the black hole's surface gravity, hence the principles of thermodynamics are satisfied [1-3].

Having the black hole temperature and entropy, one can study the black hole thermodynamics [4]. There are several kinds of black holes, the simplest one described by only one parameter which is the black hole mass, it is Schwarzschild black hole [5, 6]. A black hole carrying electric charge is known as the Reissner Nordstrom black hole and was already been examined from a thermodynamics standpoint [7]. Adding rotation to the Schwarzschild black hole yields the well-known Kerr black hole. Thermodynamics, stability, and Hawking-Page phase transition of the Kerr black hole was studied in Ref. [8]. The Kerr-Newman black hole described by three parameters; mass, electric charge, and rotation, which govern the black hole thermodynamics [9]. On the other hand, a black hole in anti-de Sitter (AdS) space is significant in terms of gauge/gravity [10, 11].

Horava-Lifshitz black holes, which are the subject of this study, are also among the most fascinating types of black holes. With general coupling constants, Horava-Lifshitz black holes admit spherically symmetric solutions. Those black holes are first constructed by Horava. Horava-Lifshitz gravity is indeed a theory of quantum gravity, which is nothing but a renormalizable non-relativistic theory of gravity. At large radii, Horava-Lifshitz black hole solutions can be reduced to Einstein's general relativity black hole, whereas at small scales they reveal violated Lorentz symmetry. In this study, we want to study the exponential correction on the thermodynamics of HoravaLifshitz black hole to find the effect of non-perturbative corrections.

### 2 Black Hole Metric

The four-dimensional Kehagius-Sfetsos (KS) solution of Horava-Lifshitz black hole is described by the following metric

$$ds^2 = f(r)dt^2 - \frac{dr^2}{f(r)} - r^2 d\Omega_2^2 \quad (1)$$

where

$$f(r) = k + \omega r^2 - \omega r^2 \sqrt{1 + \frac{4m}{\omega r^3}} \quad (2)$$

where  $m$  is the mass parameter so that black hole mass is given by  $M = am$ , where  $a$  is a positive constant. Using  $f(r) = 0$ , we find inner ( $r_-$ ) and outer ( $r_+$ ) horizons as

$$r_{\pm} = \frac{2m\omega \pm \sqrt{4\omega^2 - 2\omega k^3}}{2k\omega} \quad (3)$$

In the case of  $k = 1$ , the mass parameter is obtained as

$$m = \frac{1 + 2\omega r_+^2}{4\omega r_+} \quad (4)$$

For metric (1), the black hole temperature is given by

$$T = \frac{1}{4\pi} \left( \frac{df(r)}{dr} \right)_{r=r_+} \quad (5)$$

### 3 Thermodynamics

One of the best ways to study black holes is to study their thermodynamics. The entropy of our desired black hole is given in terms of the event horizon with the following relation

$$S_0 = \pi r_+^2 + \frac{2\pi}{\omega} \ln r_+ \quad (6)$$

This relation is also valid for many other four-dimensional black holes, while temperature is related to the surface gravity of a black hole and is obtained using the mass parameter (4) and expression (5), we can find the KS black hole temperature as follows

$$T = \frac{2\omega r_+^2 - 1}{8\pi r_+ (1 + \omega r_+^2)} \quad (7)$$

The above temperature equation demonstrates that the situation of  $\omega = 0$  results in negative temperature, which is clearly not a physical case. For the cases of  $\omega \neq 0$ , one can find a minimum value for the event horizon radius, which is henceforth symbolized by  $r_{+m}$ . Besides, at large  $r_+$ , the value of  $\omega$  has no important effect on the temperature:

$$T(r_+ \rightarrow \infty) = \frac{1}{4\pi r_+} \quad (8)$$

Since the black hole pressure is proportional to the cosmological constant, there is no variable corresponding to the thermodynamics pressure of this case. Hence, the first law of black hole thermodynamics reads

$$dE = TdS \quad (9)$$

where  $E$  is the internal energy and  $S$  is the black hole entropy, which was given in Eq. (6). To have more information about the black hole thermodynamics of KS solution, we will study the corrected thermodynamics in the next section.

### 5 Corrected thermodynamics

Corrected entropy of the KS black hole with  $k = 1$  is given by

$$S = \pi r_+^2 + \frac{2\pi}{\omega} \ln r_+ + \eta r_+^{-\frac{2\pi}{\omega}} e^{-\pi r_+^2} \quad (10)$$

Assigning the black hole mass as being identical to the uncorrected internal energy, the first law of black hole thermodynamics (9) emerges in its standard form:

$$dm = TdS_0 \quad (11)$$

Then, using the partition function, the corrected internal energy is given by

$$E = m + \eta \frac{(\omega r_+^2 + 1)(2\omega r_+^2 - 1)^2 r_+^{-\frac{2\pi + \omega}{\omega}} e^{-\pi r_+^2}}{4\omega(2\omega^2 r_+^4 - 5\omega r_+^2 - 1)} \quad (12)$$

Moreover, using the well-known relation of the Helmholtz free energy with the partition function one can obtain

$$F = \frac{(1-2\omega r_+^2) \ln r_+ + \omega^2 r_+^4 + \frac{7}{2}\omega r_+^2 + 1}{4\omega r_+(\omega r_+^2 + 1)} - \eta \frac{(\omega r_+^2 - \frac{1}{2})r_+ - \frac{2\pi}{\omega} e^{-\pi r_+^2}}{4\pi r_+(\omega r_+^2 + 1)} \quad (13)$$

Since there is no dual variable pressure, we can assume that  $P = 0$ , which yields  $H = E$ , where  $H$  denotes the enthalpy. Namely, in the absence of the non-perturbative corrections, black hole enthalpy is identical to the black hole mass. Hence, the Gibbs free energy is equal to the Helmholtz free energy. In the simplest cases, the equilibrium thermodynamics is governed by the *Gibbs free energy*, whose *global minimum* yields the state of a system for a fixed temperature. Using the fact that the mass of the black hole is interpreted as the enthalpy, we have the thermodynamics formula:  $G = M - TS$ .

The *local thermodynamic stability* is given by the positivity of the specific heat which is obtained by the following thermodynamics relation. We can see that it is negative for the Schwarzschild black hole. It means that while the Schwarzschild black hole loses its energy, then increases the temperature. So, it is thermodynamically unstable and will evaporate. However, by reducing its size due to the Hawking radiation, the scenario may be changed if we take into account the thermal fluctuations of the statistical physics or quantum corrections.

The important question now is whether this physical system has thermodynamic stability or not. To understand this, we examine the specific heat in the constant volume of the system, which is obtained from the following equation

$$C_V = T \frac{dS}{dT} \quad (14)$$

Graphical analysis is presented by Fig. 1.

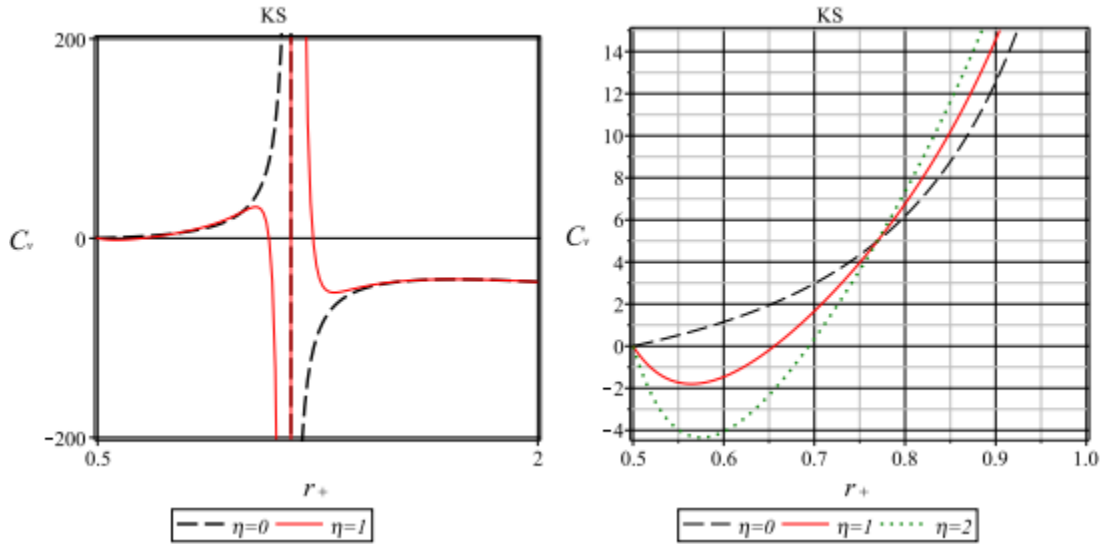


Figure 1: Specific heat in terms of event horizon (radius) of KS solution with  $\omega = 2$

It shows that the KS solution of the HL black hole is unstable at large radii, however reducing its size due to Hawking radiation translates it to the stable phase through a second-order phase transition. The effect of quantum correction is clear now by focusing on the small radii. In presence of exp correction, a black hole has negative specific heat again at infinitesimal horizon radius. So, the final stage of the KS solution of the HL black hole will be unstable which is not clear from an

ordinary classical point of view. Hence the KS black hole turns out to be unstable before stopping the radiation, which yields the complete black hole evaporation.

## 6 Conclusion

In this work, we considered the KS solutions of Horava-Lifshitz black hole to study the effect of the non-perturbative correction on the thermodynamics quantities. In fact, the KS solution was a black hole with zero cosmological constant. We found that the exponential correction of the black hole entropy affects the thermodynamics quantities of the KS solution at small radii. We showed that the specific heat analysis of the KS solution is stable by neglecting the quantum corrections while the non-perturbative corrections make the KS black hole unstable at a small horizon radius.

We showed that the non-perturbative quantum effects correct the black hole entropy with an exponential term. This is happened by the modification of the angular dependent part of the metric. Hence, it has no effect on the metric function  $f(r)$ . Therefore, the horizon radius and black hole temperature is kept unchanged.

## References

- [1] J. M. Bardeen, B. Carter and S. W. Hawking, "The four laws of black hole mechanics", *Commun. Math. Phys.* 31 (1973) 161 17
- [2] J. D. Bekenstein, "Black holes and the second law", *Lett. Nuovo Cim.* 4 (1972) 737
- [3] J. D. Bekenstein, "Black Holes and Entropy", *Phys. Rev. D* 7 (1973) 2333
- [4] S. Sarkar, "Black Hole Thermodynamics: General Relativity and Beyond", *Gen. Rel. and Grav.* 51 (2019) 63
- [5] M. Moussa, "Schwarzschild Black Hole Thermodynamics and Generalized Uncertainty Principle", *Int. J. Theor. Phys.* (2021)
- [6] D. A. Gomes, R. V. Maluf, C. A. S. Almeida, "Thermodynamics of Schwarzschild-like black holes in modified gravity models", *Annals Phys.* 418 (2020) 168198
- [7] K. Ghaderi, B. Malakolkalami, "Thermodynamics of the Schwarzschild and the Reissner-Nordstrom black holes with quintessence", *Nucl. Phys. B* 903 (2016) 10
- [8] V. G. Czinner, H. Iguchi, "Thermodynamics, stability and Hawking-Page transition of Kerr black holes from Rnyi statistics", *Eur. Phys. J. C* 77 (2017) 892
- [9] O. Ruiz, U. Molina, and P. Vilorio, "Thermodynamic analysis of Kerr-Newman black holes", *Journal of Physics: Conf. Series* 1219 (2019) 012016
- [10] V. E. Hubeny, D. Marolf, M. Rangamani, "Hawking radiation from AdS black holes", *Class. Quantum Grav.* 27 (2010) 095018
- [11] B. Pourhassan, J. Sadeghi and A. Chatrabhuti, "AdS5 black hole at N=2 supergravity" *Indian J. Phys.* 87 (2013) 691

## AdS/BCFT correspondence and BTZ black hole within electric field

Fabiano F. Santos

Instituto de Física, Universidade Federal do Rio de Janeiro, 21941-972 Rio de Janeiro, Brazil;  
email: fabian.offis23@gmail.com

### Abstract:

This paper, presents the gravity duals of Conformal Field Theories with boundaries. This theory is known as AdS/BCFT correspondence. In this duality, our system has 3D gravity coupling with the Maxwell field dual to 2D BCFT. On the gravity side, we consider a 3D BTZ black hole. We analyze the effects of the chemical potential on the profile of the extra boundary for the black hole. Performing a holographic renormalization, we calculate the free energy and obtain the total entropy and corresponding area with chemical potential, and the boundary entropy for the black hole. These theories are specified by stress-energy tensors that reside on the extensions of the boundary to the bulk. In this way, the AdS/BCFT appears analogous to the fluid/gravity correspondence with the chemical potential. We discuss the solutions as well as their thermodynamic and fluid properties.

Keywords: AdS<sub>3</sub>/BCFT<sub>2</sub> correspondence; Electric field; fluid/gravity correspondence.

# Part Four

## Poster Presentations

## Travelling wave solution of Balitsky-Kovchegov equation

Ranjana Saikia<sup>1</sup>, Pragyana Phukan<sup>2</sup>, Jayanta Kumar Sarma<sup>3</sup>

<sup>1</sup>Department of Physics, Tezpur University, Tezpur, Assam, 784028, India

Email: ranjans@tezu.ernet.in

<sup>2</sup>Department of Physics, Moran College, Moranhat, Assam, 785670, India

Email: pragyana@morancollege.com

<sup>3</sup>Department of Physics, Tezpur University, Tezpur, Assam, 784028, India

Email: jks@tezu.ernet.in

**Abstract.** In this work, we suggest an approximate analytical solution of the Balitsky-Kovchegov (BK) equation in momentum space using a method called the homotopy perturbation method (HPM). With some change of variables and the truncation of the BFKL (Balitsky-Fadin-Kuraev-Lipatov) kernel, the BK equation in momentum space can be transformed into the FKPP (Fisher-Kolmogorov-Petrovsky-Piscounov) equation. Observed geometric scaling at small- $x$  at HERA and travelling wave solution of the FKPP equation are similar. The solution of the BK equation obtained in this work also suggests the travelling wave nature of the measured scattering amplitude  $N(k, Y)$  plotted at various rapidities. The solution obtained in his work can be helpful in further phenomenological studies at high-density QCD.

Keywords: Parton saturation, BK equation, Travelling wave solution

## 1 Introduction

One of the most important phenomena of QCD at high energies or equivalently at small- $x$  (Bjorken  $x$ ) is the growth of hadronic cross-sections. Hadronic cross-sections have been incited by states with high partonic densities at small- $x$ . Many theoretical and phenomenological efforts have been made to understand and explain the high-density QCD at small- $x$ . Let us talk only about gluon densities at very small- $x$  as one can neglect quark densities there. The fast growth of gluons at small- $x$  is well described by the BFKL equation [1, 2]. This equation can be derived with perturbative QCD (pQCD) by resumming leading logarithms of energies expressed in terms of  $x$  such as  $\ln(1/x) \gg \ln(Q^2/\mu^2)$ , where  $Q$  and  $\mu$  being the photon virtuality and renormalization scale respectively. It is seen from the solution of the BFKL equation that the measured scattering amplitude  $N(k, Y)$  ( $k$  being the transverse momentum and  $Y$  being the rapidity of evolved gluons) and hence the total cross-section exhibits an exponential growth with rapidity  $Y$ . At very small- $x$ , the rapidly increased gluon densities need to be tamed down to hold the unitarity and hence Froissart-Martin bound [3]. Froissart-Martin bound says, the total cross-section of a given process cannot grow faster than the logarithm of energy squared. Thus, at very small  $x$  or high energies, the BFKL equation violates the unitarity and hence Froissart-Martin bound. So, its applicability is limited and cannot be used at arbitrarily high energies.

The above problems faced by the BFKL equation are to be addressed to understand the physics at small- $x$ . The solution is that at high energies or small- $x$ , gluons themselves start to recombine and get saturated finally. The first idea of gluon-gluon recombination is addressed in ref. [4-8]. The gluon-gluon recombination will tame down the gluon density and saturation of gluons will solve the unitarity problem. BFKL equation, being linear, could not address the nonlinear effect of gluon recombination and saturation and hence is unable to explain implicit physics at high-density QCD.

It is imperative to understand the implicit physics in the saturation region of gluons at small- $x$ . In this region, linear QCD evolution equations are replaced by the nonlinear QCD evolution equations, helping to understand the gluon-gluon recombination and saturation effect. The nonlinear evolution equations have important features dealing with the saturation effect as they contain damping terms that reflect the saturation effect arising out of gluon-gluon recombination. The Jalilian-Marian-Iancu-McLerran-Weigert-Leonidov-Kovner (JIMWLK) equation [9-12] permits gluon saturation in high-density gluon region at small- $x$  that addresses the nonlinear correction using the Wilson renormalization group approach. However, it is complicated to solve the JIMWLK equation because of its complex nature, and hence unable to apply it in phenomenological studies. Instead, its mean field approximation BK equation [13-16] is studied most in the context of saturation effect. Though, it is tough to solve the BK equation using general methods. BK equation is an integrodifferential equation in coordinate space that can be transformed into momentum space resulting in a partial differential equation. Analytical solutions to the BK equation proposed recently with different approaches using some approximations can be found in ref. [17-22]. These analytical solutions shed light on the ability of the BK equation in explaining gluon saturation and its application in the high-energy hadron scattering phenomena.

In this work, we suggest an approximate analytical solution to the BK equation using the homotopy perturbation method (HPM) [23, 24]. The BK equation in momentum space with some change of variables and truncation of the BFKL kernel can be transformed into the Fisher-Kolmogorov-Petrovsky-Piscounov (FKPP) equation [17-19]. The FKPP equation [25, 26] is a partial differential equation that belongs to the reaction-diffusion equation in statistical physics. Observed geometric scaling phenomena at small- $x$  at HERA can be related to the travelling wave solution of the FKPP equation [27]. The transition of the scattering amplitude into the saturation region is similar to the formation of the front of the travelling wave of the FKPP equation [17]. We obtain the solution of the BK equation which also suggests the travelling wave nature of the solution. The solution of the BK equation obtained in this work can be helpful for further phenomenological studies in light of present and future accelerator facilities.

We organize the paper as follows. In section 2, we discuss the relation between the BK and the FKPP equations. The solution of the BK equation is presented in section 3. The summary and conclusion are presented in section 4.

## 2 Relation between the BK and FKPP equations

The relation between the BK and FKPP equations has been found in the pioneering work done by S. Munier and R. B. Peschanski [17-19]. In this section, we discuss how to relate the BK equation with the FKPP equation following their work.

BK equation is about energy dependence of scattering amplitude at small- $x$ , it is often convenient to carry out work in the pQCD dipole picture of deep inelastic scattering (DIS) [28-31]. This picture is known as the dipole model, which is valid at small- $x$ . The main advantage of the dipole picture of DIS is the factorization of the scattering process into several steps, resulting in smooth use of pQCD. In the dipole picture, an incoming virtual photon after fluctuation changes to a quark-antiquark dipole. The quark-antiquark pair then scattered off the target proton and recombines to form some final state particles. In reference to the dipole picture of DIS, in the leading logarithm approximation of pQCD, the cross-section in terms of the total rapidity ( $Y$ ) and the virtuality of the photon ( $Q$ ) factorizes to [27]

$$\sigma^{\gamma^*p} = \int_0^\infty x_{01} dx_{01} \int_0^1 dz |\psi(z, x_{01}Q)|^2 N(Y, x_{01}), \quad (1)$$

where  $z$  being the longitudinal momentum fraction of the quark of the virtual photon,  $\psi(z, x_{01}Q)$  is the photon wave function on a quark-antiquark dipole of its size  $x_{01}$ .  $N(Y, x_{01})$  is the forward dipole-proton scattering amplitude.

Within the large  $N_c$  approximation at fixed coupling and for a homogeneous nuclear target, the measured scattering amplitude  $N(k, Y)$  at transverse momentum  $k$  and total rapidity  $Y$  obeys the BK equation in momentum space given by [15]

$$\partial_Y N = \bar{\alpha} \chi(-\partial_L) N - \bar{\alpha} N^2, \quad (2)$$

where  $\bar{\alpha} = \frac{\alpha_s N_c}{\pi}$  and  $\chi(\zeta) = 2\psi(1) - \psi(\zeta) - \psi(1 - \zeta)$  is the BFKL kernel.  $\zeta = -\partial_L$ , where  $L = \ln\left(\frac{k^2}{k_0^2}\right)$ ,  $k_0$  being some low momentum scale at fixed. The expansion of the BFKL kernel around  $\zeta = \frac{1}{2}$  has been suggested in ref. [17], and with this expansion equation (2) reduces to the nonlinear partial differential equation given by

$$\partial_Y N = \bar{\alpha} \bar{\chi}(-\partial_L) N - \bar{\alpha} N^2, \quad (3)$$

where

$$\bar{\chi}(-\partial_L) = \chi\left(\frac{1}{2}\right) + \frac{\chi''\left(\frac{1}{2}\right)}{2} \left(\partial_L + \frac{1}{2}\right)^2. \quad (4)$$

In reference to the above expansion and defining  $\bar{\zeta} = 1 - \frac{1}{2} \sqrt{1 + 8 \frac{\chi\left(\frac{1}{2}\right)}{\chi''\left(\frac{1}{2}\right)}}$ , with the following change of variables [17]

$$t = \frac{\bar{\alpha} \chi''\left(\frac{1}{2}\right)}{2} (1 - \bar{\zeta})^2 Y, \quad x = (1 - \bar{\zeta}) \left( L + \frac{\bar{\alpha} \chi''\left(\frac{1}{2}\right)}{2} Y \right),$$

$$u(t, x) = \frac{2}{\chi''\left(\frac{1}{2}\right) (1 - \bar{\zeta})^2} N \left( \frac{2t}{\bar{\alpha} \chi''\left(\frac{1}{2}\right) (1 - \bar{\zeta})^2}, \frac{x}{(1 - \bar{\zeta})} - \frac{t}{(1 - \bar{\zeta})^2} \right),$$

the equation (3) turns into the FKPP equation for  $u(t, x)$ , can be expressed as [17]

$$\partial_t u(t, x) = \partial_x^2 u(t, x) + u(t, x) - u^2(t, x). \quad (5)$$

Thus, with some change of variable transformation, it is seen that the BK equation (3) can be transformed to the above equation (5), which is the famous FKPP equation.

### 3 Solution of the BK equation with HPM

Given the discussion of the relation between the FKPP and the BK equations discussed in the previous section, let us solve the BK equation for the scattering amplitude  $N(k, Y)$ . The solution of the BK equation (3) in connection with the equation (5) for the scattering amplitude  $N(k, Y)$  using the HPM can be written as

$$N(k, Y) = \frac{N_0 e^Y}{1 - N_0 + N_0 e^Y}, \quad (6)$$

where  $N_0$  is the initial condition. Once the initial condition is known to us, the solution of the BK equation gives the scattering amplitude  $N(k, Y)$  at any given rapidity  $Y > 0$ . In this work, we will use the following initial condition given by K. Golec-Biernat and M. Wusthoff (GBW), introduced first in ref. [32]

$$N^{GBW}(r, Y = 0) = 1 - \exp\left[-\left(\frac{r^2 Q_{s0}^2}{4}\right)\right]. \quad (7)$$

$Q_{s0}^2$  is the fit parameter, called the initial saturation scale squared. This initial condition can simply be Fourier transformed into momentum space analytically and applied to the BK equation in momentum space. The momentum space result of the GBW initial condition can be written as

$$\begin{aligned} N^{GBW}(k, Y = 0) &= \int \frac{d^2 r}{2\pi r^2} e^{ik \cdot r} N^{GBW}(r, Y = 0) \\ &= \frac{1}{2} \Gamma\left(0, \frac{k^2}{Q_{s0}^2}\right). \end{aligned} \quad (8)$$

$\Gamma(0, k^2/Q_{s0}^2)$  is the incomplete gamma function. At large values of  $k^2/Q_{s0}^2$ , this behaves as

$$\Gamma\left(0, \frac{k^2}{Q_{s0}^2}\right) = \exp\left(-\frac{k^2}{Q_{s0}^2}\right).$$

Therefore,

$$N^{GBW}(k, Y = 0) = \frac{1}{2} \exp\left(-\frac{k^2}{Q_{s0}^2}\right). \quad (9)$$

Substitution of the above equation in equation (6) for the initial condition  $N_0$ , we obtain the scattering amplitude  $N(k, Y)$  with GBW as the initial condition

$$N(k, Y) = \frac{e^{Y - k^2/Q_{s0}^2}}{1 - e^{-k^2/Q_{s0}^2} + e^{Y - k^2/Q_{s0}^2}}. \quad (10)$$

This is the approximate analytical solution of the BK equation (3). The evolution of the scattering amplitude at different rapidities can be seen in Fig. 1

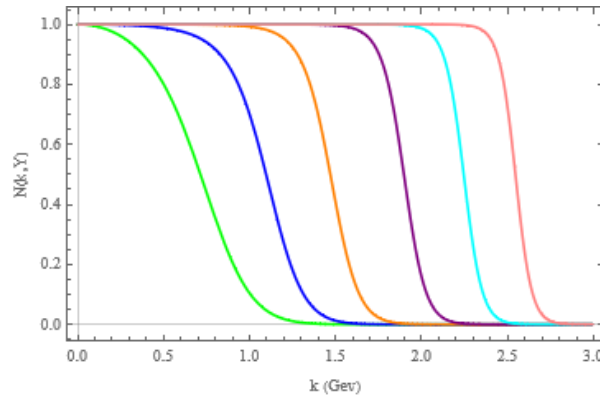


Figure 23. The solution of the BK equation in momentum space,  $N(k)$ , at various rapidities  $Y = 2$ ,  $Y = 5$ ,  $Y = 9$ ,  $Y = 15$ ,  $Y = 21$  and  $Y = 27$ .

#### 4 Summary and conclusion

This work has suggested an approximate analytical solution of the BK equation using the HPM. The relation between the geometric scaling phenomena of the solution of the BK equation and the travelling wave solution of the FKPP equation, as suggested by S. Munier and R. Peschanski in their pioneering work, has guided the scientific community working in the field of gluon saturation. In this work, we have started our discussion with the relation between the BK and FKPP equations. We carried out work in the pQCD dipole picture of DIS in which the measured scattering amplitude  $N(k, Y)$  obeys the BK equation in the momentum space frame to work in the context of at least travelling wave solution and the geometric scaling. Afterward, with some change of variables and a slight approximation in the BK equation, we ended with the approximated analytical solution of the BK equation in the momentum space. We plotted the obtained solution, equation (10), at different rapidities in Fig. 1 to check the travelling wave nature of the solution. Indeed, one can see the solution's travelling wave nature. It indicates that at high energies, the scattering amplitude behaves as a wave travelling from the region  $N = 1$  to  $N = 0$  as  $k$  increases without being changed in the profile. It is indeed a vital physical result of this travelling wave approach.

The solution obtained in this work can be helpful in further phenomenological studies in high-density QCD and saturation regions. However, it is going to be interesting to observe whether this type of travelling wave solution and geometric scaling exist or not at very high energies when EIC (Electron-Ion-Collider) [33] and other future projects run operations. Nevertheless, the BK equation with truncation of the BFKL kernel successfully explains the observed geometric scaling and the travelling wave nature of its solution at current accelerator facilities. We must rely on the future acceleration facilities for precise measurements of observed phenomena and their confirmation.

#### References

- [1] E. Kuraev, L. Lipatov, and V. Fadin, “The pomeron singularity in nonabelian gauge theories”, *Sov. Phys. JETP* 45, 3 (1977).
- [2] Y. Y. Balitsky, and L. Lipatov, “The pomeron singularity in quantum chromodynamica”, *Yad. Fiz.* 28, 1597 (1978).
- [3] M. Froissart, “Asymptotic behavior and subtractions in the mandelstam representation”, *Physical Review* 123 (3), 1053 (1961).
- [4] L. Gribov, E. Levin, and M. Ryskin, “Singlet structure function at small  $x$ : Unitarization of gluon ladders”, *Nuclear Physics B* 188 (3), 555 (1981).
- [5] L. V. Gribov, E. M. Levin, and M. G. Ryskin, “Semihard processes in QCD”, *Physics Reports* 100 (1-2) 1 (1983).
- [6] A. H. Mueller, and J. Qiu, “Gluon recombination and shadowing at small values of  $x$ ”, *Nuclear Physics B* 268 (2) 427 (1986).
- [7] A. H. Mueller, “Small- $x$  behavior and parton saturation: A QCD model”, *Nuclear Physics B* 335 (1) 115 (1990).
- [8] W. Zhu, and J. Ruan, “A new modified altarelli-parisi evolution equation with parton recombination in proton”, *Nuclear Physics B* 559 (1-2) 378 (1999).
- [9] I. Balitsky, “Operator expansion for high-energy scattering”, *Nuclear Physics B* 463 (1) 99 (1996).
- [10] J. Jalilian-Marian, A. Kovner, A. Leonidov, and H. Weigert, “The BFKL equation from the Wilson renormalization group”, *Nuclear Physics B* 504 (1-2) 415 (1997).
- [11] E. Iancu, A. Leonidov, and L. McLerran, “Nonlinear gluon evolution in the color glass condensate: I”, *Nuclear Physics A* 692 (3-4) 583 (2001).
- [12] H. Weigert, “Unitarity at small bjorken  $x$ ”, *Nuclear Physics A* 703 (3-4) 823 (2002).
- [13] I. Balitsky, “Operator expansion for diffractive high-energy scattering”, in: *AIP Conference Proceedings*, Vol. 407, American Institute of Physics, 953 (1997).
- [14] Y. V. Kovchegov, “Small- $x$   $F_2$  structure function of a nucleus including multiple pomeron exchanges”, *Physical Review D* 60 (3) 034008 (1999).
- [15] Y. V. Kovchegov, “Unitarization of the BFKL pomeron on a nucleus”, *Physical Review D* 61 (7) 074018 (2000).
- [16] I. Balitsky, “Effective field theory for the small- $x$  evolution”, *Physics Letters B* 518 (3-4) 235 (2001).
- [17] S. Munier, and R. Peschanski, “Geometric scaling as traveling wave”, *Physical Review Letters* 91 (23) 232001 (2003).
- [18] S. Munier, and R. Peschanski, “Traveling wave fronts and the transition to saturation”, *Physical Review D* 69 (3) 034008 (2004).
- [19] S. Munier, and R. Peschanski, “Universality and tree structure of high-energy QCD”, *Physical Review D* 70 (7) 077503 (2004).
- [20] W. Xiang, S. Cai, and D. Zhou, “Approximate solution to the NLL BK equation in the saturation region”, *Physical Review D* 95 (11) 116009 (2017).
- [21] W. Xiang, Y. Cai, M. Wang, and D. Zhou, “High-energy asymptotic behavior of the S matrix in the saturation region with the smallest dipole running coupling prescription”, *Physical Review D* 101 (7) 076005 (2020).
- [22] X. Wang, Y. Yang, W. Kou, R. Wang, and X. X. Chen, “Analytical solution of Balitsky-Kovchegov equation with homogeneous balance method”, *Physical Review D* 103 (5) 056008 (2021).

- [23] J.-H. He, “Homotopy perturbation technique”, *Computer methods in applied mechanics and engineering* 178 (3-4) 257 (1999).
- [24] J.-H. He, “A coupling method of a homotopy technique and a perturbation technique for non-linear problems”, *International journal of non-linear mechanics* 35 (1) 37 (2000).
- [25] R. A. Fisher, “The wave of advance of advantageous genes”, *Annals of eugenics* 7 (4) 355 (1937).
- [26] P. Kolmogorov, and Piskunov, “A study of the diffusion equation with increase in the amount of substance, and its application to a biological problem”, *Bull. Moscow Univ. Math. Mech.* 1.
- [27] A. Stasto, K. Golec-Biernat, and J. Kwiecinski, “Geometric scaling for the total  $\gamma^*p$  cross section in the low x region”, *Physical Review Letters* 86 (4), 596 (2001).
- [28] N. N. Nikolaev, and B. Zakharov, “Color transparency and scaling properties of nuclear shadowing in deep inelastic scattering”, in: *30 years Of The Landau Institute- Selected Papers*, World Scientific, 733 (1996).
- [29] A. H. Mueller, “Soft gluons in the infinite-momentum wave function and the BFKL pomeron”, *Nuclear Physics B* 415 (2), 373 (1994).
- [30] A. H. Mueller, and B. Patel, “Single and double BFKL pomeron exchange and a dipole picture of high energy hard processes”, *Nuclear Physics B* 425 (3), 471 (1994).
- [31] A. H. Mueller, “Unitarity and the BFKL pomeron”, *Nuclear Physics B* 437 (1), 107 (1995).
- [32] K. Golec-Biernat, and M. Wusthoff, “Saturation effects in deep inelastic scattering at low  $Q^2$  and its implications on diffraction”, *Physical Review D* 59 (1), 014017 (1998).
- [33] A. Accardi, J. Albacete, et al., “Electron-ion collider: The next QCD frontier”, *The European Physical Journal A* 52 (9), 1 (2016).

## Dirac particle near R - N black hole, quasinormal mode and harmonic oscillator energy

Mohammad Reza Alipour<sup>1</sup>, Jafar Sadeghi<sup>1</sup>

<sup>1</sup> Department of Physics, Faculty of Basic Sciences, University of Mazandaran P. O. Box 47416-95447, Babolsar, Iran.

Email: mr.alipour@stu.umz.ac.ir

Email: pouriya@ipm.ir

**Abstract.** In this paper, we try to study the behavior of the Dirac particle in the background of the Rosener Nordstrom black hole and try to obtain its energy spectrum and we will examine it. Also use energy spectrum to obtain the entropy and particle information close to the event horizon.

Keywords: Dirac equation, Entropy, Energy spectrum, R - N black hole

### 1 Introduction

One of the successes of general relativity is the mysterious physical prediction of the black hole in the universe, for this reason, theoretical physics has been studying the black hole for decades. Also, black holes are one of the quantum phenomena due to Hawking radiation. So black holes can help us understand the relationship between general relativity theory and quantum mechanics. We consider the theory of quantum fields in curved space-time and the behavior of different fields interacting with the gravitational field to construct a theory that incorporates both quantum mechanics and general relativity [1, 2]. That's why black holes are being studied to obtain information and its implications are mentioned in these articles [3, 4, 5]. Black holes have three observable quantities, mass, electric charge and angular momentum, where are divided into different categories. The black hole with a charge and mass is called a Reissner-Nordstrom black hole, similar to the Schwarzschild black hole but with two outer and inner event horizons. So, in the limit ( $Q \rightarrow 0$ ) we will have the same Schwarzschild black hole also in the limit of ( $Q \rightarrow M$ ) will have extreme Reissner-Nordstrom black hole. When we solve a scalar or Dirac field in the curve space, get to imaginary energy that is first time the term quasi normal mode used by Simone and Will and Fiziev [6, 7], which is an interesting property and plays an important role. He plays in black hole physics. The quasinormal state for black holes also produces a set of discrete frequencies and is made up of two real and imaginary parts, we whose real part corresponds to the actual frequency and its imaginary part is proportional to the attenuation rate when ( $\omega_I > 0$ ). It decreases from the oscillator, and when it is ( $\omega_I < 0$ ) it indicates instability. The quasinormal modes provide a unique opportunity for black hole recognition. Hopefully in the near future large-scale interferometric detectors will be exploited to detect gravitational waves. In order to extract as much information as possible from the gravitational wave signal it is important that we achieve how the quasinormal modes depend on the black hole parameters. According to the article [8] we considered the Klein-Gordon particles near the Reissner-Nordstrom black hole and obtained its entropy and also showed that each particle contains 8 bits of information stored on the black hole. Now in this paper, we want to investigate the Dirac particles near the Reissner-Nordstrom black hole and investigated entropy and thermal property black hole. All above information give us

motivation to investigate following section: In section 2, we introduce the Reissner-Nordstrom black hole. In section 3, write the Dirac equation in curve space-time. In section 4, we employ the particle on Reissner-Nordstrom black hole and obtain the energy and wave function in near Reissner-Nordstrom black hole. In section 5, we calculate thermal properties of Reissner-Nordstrom black hole with energy spectrum and finally, we explain the result in section 6.

### Reissner-Nordstrom black hole

The Reissner-Nordstrom black hole is described by two observable quantities  $Q$  and  $M$ , the metric being written as follows [9]

$$ds^2 = f(r)dt^2 - \frac{1}{f(r)} dr^2 - r^2 d\theta^2 - r^2 \sin^2 \theta d\varphi^2 \quad (1)$$

This is achieved by placing  $f(r) = 0$ , two outer and inner event horizons for the black hole, where  $f(r)$  can be written in terms of outer and inner  $r_{\pm} = M \pm \sqrt{M^2 - Q^2}$  event horizons

$$f(r) = \frac{(r-r_+)(r-r_-)}{2} \quad (2)$$

### Dirac equation in curve space-time

As we know, the Dirac equation of spin  $\frac{1}{2}$  particles are invariant under the Lorentz transformation. So in Minkowski at space-time, we have the following equation

$$(i \gamma^a \partial_a - m) \Psi = 0 \quad (3)$$

where  $\gamma^a$  is the standard Dirac matrix  $4 \times 4$  in space-time and is shown below in terms of Pauli  $\sigma_i$ ,  $i = 1, 2, 3$  and unit matrices  $I_{2 \times 2}$

Now, we use the covariant derivative and the tetrad representation, the Dirac equation in curved space-time will be following

$$g_{\mu\nu} = e_{\mu}^a e_{\nu}^b \eta_{ab} \quad (4)$$

where  $\eta_{ab}$  and  $g_{\mu\nu}$  are at and curved tensor space-time respectively. Thus, the Dirac equation in curved space-time with electromagnetism can be written by

$$(i \gamma^{\mu} D_{\mu} - m) \Psi = 0 \quad (5)$$

and

$$D_{\mu} = \partial_{\mu} + \Gamma_{\mu} + ie A_{\mu} \quad \Gamma_{\mu} = \frac{1}{4} \omega_{\mu}^{ab} \gamma_{ab} \quad (6)$$

Also,  $\omega_{\mu}^{ab}$  and  $\gamma_{ab}$  can be obtained as follows,

$$\gamma_{ab} = \frac{1}{2} [\gamma_a, \gamma_b] \quad \omega_{\mu}^{ab} = e_{\nu}^a \Gamma_{\sigma\mu}^{\nu} e^{\sigma b} - e^{\nu b} \partial_{\mu} e_{\nu}^a \quad \gamma^{\mu} = e_a^{\mu} \gamma^a \quad (7)$$

where  $\Gamma_{\sigma\mu}^{\nu}$  is Christoffel symbol.

### Energy spectrum of particle near the proximity Reissner-Nordstrom black hole

According equations also, when  $A_{\mu} = (\frac{Q}{r}, 0, 0, 0)$  ( $Q$  is charged black hole) and consider the wave

function as  $\Psi = \frac{e^{-iEt}}{r f^{\frac{1}{4}}(r) \sin^2 \theta} \psi$ , Dirac equation is obtained as following

$$[\gamma^0 f^{-\frac{1}{2}}(r)E + i\gamma^1 f^{\frac{1}{2}}(r)\partial_1 + \frac{i\gamma^2}{r}\partial_2 + \frac{i\gamma^3}{r \sin\theta}\partial_3 - \gamma^0 f^{-\frac{1}{2}}(r)\frac{qQ}{r} - m]\psi = 0 \quad (8)$$

For the spherical part deformation operator  $K$  [12]:

$$K = \gamma^0 \gamma^1 \left( \gamma^2 \partial_2 + \frac{\gamma^3 \partial_3}{\sin\theta} \right) \quad K\psi = k\psi \quad (9)$$

where  $k = 0, \pm 1, \pm 2, \dots$  is eigenvalues of operator  $K$ . So, the spherical part  $Z(\theta, \phi)$  and  $\psi$  will be following

$$\psi = Z(\theta, \phi) \begin{pmatrix} g(r) \\ ih(r) \end{pmatrix} \quad (10)$$

where  $I_2 = \begin{pmatrix} 1 \\ 1 \end{pmatrix}$  in this case, separated we get two separate equations for the radial part by

Considering this equation near the outer event horizon ( $r \rightarrow r_+$ ), and taking into account

$$p = \left( \frac{r_-}{r_+} - 1 \right)^{-\frac{1}{2}}, \quad y = \left( 1 - \frac{r}{r_+} \right)^{\frac{1}{2}} \text{ one can calculate}$$

$$y \frac{dh}{dy} + 2kyp h(r) - 2p r_+ \left[ p \left( E - \frac{qQ}{r_+} \right) - my \right] g(r) = 0 \quad (11)$$

$$y \frac{dg}{dy} + 2kyp g(r) + 2p r_+ \left[ p \left( E - \frac{qQ}{r_+} \right) + my \right] h(r) = 0 \quad (12)$$

When we solve the equation for the massless Dirac particle  $m = 0$ , we get following solutions [65],

$$g(y) = e^{-2kpy} y^{i\alpha} L_n^\alpha(4ikpy) \quad (13)$$

Also by using  $\omega = \frac{r_+ - r_-}{2r_+^2}$  we have

$$\alpha = \frac{2}{\omega} \left( E - \frac{qQ}{r_+} \right) \quad n = \frac{1}{\omega} \left( E - \frac{qQ}{r_+} \right) - \frac{1}{2} + i \quad (14)$$

and

$$h(y) = e^{-2kpy} y^{i\alpha} L_n^\alpha(4kpy) \quad (15)$$

where

$$\alpha = \frac{2i}{\omega} \left( E - \frac{qQ}{r_+} \right) \quad n = \frac{i}{\omega} \left( E - \frac{qQ}{r_+} \right) \quad (16)$$

We choose the wave function that decreases at a constant damping rate, so the energy spectrum (14) is considered as particle energy near the R-N black hole. Then use energy to obtain the entropy and thermal properties of the black hole.

### Thermal properties of Reissner-Nordstrom black hole with energy spectrum

We consider  $N$  particles near Reissner-Nordstrom black hole also use energy particle and partition function to obtain entropy and thermal properties of the black hole. So, we compute the partition function for  $N$  indefinite particles in the canonical set as follows [14]:

$$Z = \frac{Q^N}{N!} \quad (17)$$

and use of energy spectrum (14) to obtain  $Q$ :

$$Q = \sum_{n=0}^{\infty} e^{-\beta E_n} = e^{-\frac{\beta qQ}{r_+}} e^{i\beta\omega} \sum_{n=0}^{\infty} e^{-\beta(n+\frac{1}{2})\omega} \quad (18)$$

where  $\beta$  is invert temperature ( $\beta = \frac{1}{T}$ ). We chose real part of  $e^{i\beta\omega} = \cos(\beta\omega) + i \sin(\beta\omega)$  and note that the average energy and use Eqs. (17) and (18), we will arrive at following average value of energy:

$$\langle E \rangle = -\frac{\partial \ln Z}{\partial \beta} = \frac{N\omega}{2} + \frac{N\omega e^{-\beta\omega}}{1-e^{-\beta\omega}} + \frac{NqQ}{r_+} + N\omega \tan(\beta\omega) \quad (19)$$

We can also obtain the heat capacity directly using the average energy by the following formula:

$$C = \frac{\partial \langle E \rangle}{\partial T} = \frac{N\omega^2}{T^2} \left[ \frac{e^{-\frac{1}{T}\omega}}{(1-e^{-\frac{1}{T}\omega})^2} - \frac{1}{\cos^2(\frac{1}{T}\omega)} \right] \quad (20)$$

As can be seen in the above equation, at high temperatures the heat capacity is equal to the constant number of particles. We obtain the entropy using the average energy and the partition function as follows [14]:

$$S = \ln z + \beta \langle E \rangle \quad (21)$$

Now, we calculated entropy with consider the following Stirling's approximation ( $\ln N! = N \ln N - N$ ) and use Eqs. (17), (18), (19) and (21), so we have the following

$$S = N\beta\omega \frac{e^{-\beta\omega}}{1-e^{-\beta\omega}} - N \ln(1 - e^{-\beta\omega}) + N \ln(\cos \beta\omega) + N\beta\omega \tan(\beta\omega) - N \ln N + N \quad (22)$$

### Holography and information theory

As we know the boundary of curve as R-N black hole play important role in holography and AdS/CFT. Here, also one can think about the boundary of R-N black hole as a storage device for information. Assuming that the holographic principle holds, the maximal storage space, or total number of bits, is proportional to the area  $A$ . Let us denote the number of used bits by  $N_0$ , it is natural to assume that this number will be proportional to the area [15]. We know from the holographic principle that all information about an object is stored on its surface. It also states that a bit of information is stored in an area the length of Planck. For the black hole, its information is stored on its boundary and we use the event horizon area to describe its feature. In this section, we want to find how particles are stored near the black hole of the R - N black hole event on the surface of the black hole event horizon. First, we obtain the maximum entropy in  $N$  of Eq. (22),

$\frac{\partial S}{\partial N} = 0$  as follows:

$$S_{max} = N \quad (23)$$

Given the particles near the event horizon, we can consider the number of particles proportional to the surface of the black hole

$$A = q N \quad (24)$$

where  $q$  is a constant value. Also, we can set the maximum entropy equal to the Bekenstein entropy

$$S_{max} = S_{BH} \text{ and } S_{BH} = \frac{A}{4} [16, 17]. \text{ In this case, according to the Eqs. (23) and}$$

(24),  $q = 4$  is obtained. According to Verlinde's theory [15], each surface can be considered as information bits, so we consider the surface of the black hole as a set of information bits and write its relation as follows:

$$A = N_0 \quad (25)$$

Given the Eqs.(24) and (25), we obtain the relation of the particle number to the information bits as follows:

$$N_0 = 4 N \quad (26)$$

It shows that each particle in near R - N black hole has 4 bit of information.

### **discussion and result**

In this article, we examined the behavior of the Dirac particle and , the behavior of the Klein Gordon particle in the background of the Klein Gordon black hole in Article [8]. We came to this conclusion by comparing these two articles. For Klein Gordon particles, the energy obtained was real and in the form of a harmonic oscillator, but for Dirac particles, the energy was real and imaginary, and the real part was in the form of a harmonic oscillator plus an additional sentence.

### **Conclusions**

We used holography and found that each Klein Gordon particle contained eight bits of information on the surface of the Nordstrom Resener black hole, while the Dirac particle contained four bits of information. One of the factors that makes Dirac particle less information than Klein Gordon particle wind can be the principle of Paula's exclusion.

### **References**

- [1] F. Federici, C. Cherubini, S. Succi and M. P. Tosi, Phys. Rev. A 73, 033604 (2006).
- [2] T. R. Slatyer and C. M. Savage, Class. Quantum Grav. 22, 3833 (2005).
- [3] S. A. Fulling, Aspects of Quantum Field Theory in Curved Space-Time (Cambridge University Press, New York, 1989).
- [4] N. D. Birrell and P. C. W. Davis, Quantum Fields in Curved Space (Cambridge University Press, New York, 1994).
- [5] H. S. Vieira, V. B. Bezerra and G. V. Silva, Ann. Phys. (NY) 362, 576 (2015).
- [6] L. E. Simone and C. M. Will, Class. Quantum Grav. 9, 963 (1992).
- [7] P. P. Fiziev, Class. Quantum Grav. 23, 2447 (2006).
- [8] J. Sadeghi and M. R. Alipour, International Journal of Modern Physics A, 34, 1950196 (2019).
- [9] S. Chandrasekhar, The Mathematical Theory of Black Holes, (Oxford University Press), New York, (1983).
- [10] B. Thaller, The dirac equation, Springer Science and Business Media, (2013).
- [11] D.R. Brill and J.A. Wheeler, Rev. Mod. Phys. 29, 465 (1957).
- [12] V.I. Dokuchaev and Yu.N. Eroshenko, J. Exp. Theor. Phys. 117, 72 (2013).
- [13] J. Sadeghi, Eur. Phys. J. B 50, 453 (2006).
- [14] R. K. Pathria and P. D. Beale, Statistical Mechanics (Third Edition), Elsevier Ltd, (2011).
- [15] E. Verlinde, J. High Energy Phys. 2011, 29 (2011).
- [16] J. D. Bekenstein, Black Holes and Entropy, Phys. Rev. D 7, 2333 (1973).
- [17] J. D. Bekenstein, Bekenstein-Hawking entropy, Scholar- pedia 3, 7357 (2008).

## Constant-roll inflation in the deformed phase space scenario

S. Noori Gashti<sup>1</sup>

<sup>1</sup> Department of Physics, Faculty of Basic Sciences, University of Mazandaran P. O. Box 47416-95447, Babolsar, Iran.

Email: saeed.noorigashti@stu.umz.ac.ir

**Abstract.** This paper's primary purpose of this study is to investigate the constant-roll inflationary scenario with anisotropic conditions concerning the Einstein-æther Scalar-tensor Cosmology in noncommutative phase space. Hence, we present the point-like Lagrangian, which represents the field equations of the Einstein-æther Scalar-tensor model. According to the constant-roll conditions, we take the anisotropic constant-roll inflationary scenario in noncommutative phase space and calculate some cosmological parameters of the mentioned model, such as the Hubble parameter, potential, etc.

Keywords: constant-roll inflationary scenario, Noncommutative parameter

### 1 Introduction

One of the most famous problems researchers try to solve with different theories is quantum gravity. A common feature that can be found in all topics related to quantum gravity is called the Lorentz violation [1]. However, various gravitational models facing the Lorentz violation have recently received much attention [2–3]. One of the theories of gravity that has received much attention in connection with Lorentz's violate is called the Einstein-æther theory [4]. There exist quantities of the unitary time-like vector field, the æther field. In the Einstein-Hilbert action Integral Selecting, this field violates Lorentz symmetry in the preferred frame. The limitation of Einstein's General Relativity lives while the preservation of locality and covariance formulation is guaranteed in Einstein-æther theory. The mentioned theory, Einstein-æther theory, is called a second-order theory, used to describe different gravitational systems [5]. Einstein-æther theory has many features, and the cosmological applications of this theory have been widely discussed in the literature, including the description of the classical limit of Horava-Lifshitz. Of course, the critical point here is that the opposite is impossible [6]. Of course, from another point of view, scalar fields play a vital role in describing the universe. The field used to describe the early acceleration era of the universe is known as the inflaton field. In addition, scalar fields play a significant role in explaining the late-time acceleration as the solution to the dark energy problem. This paper aims to present a new challenge that has not been explored, namely the constant-roll inflationary scenario for the Einstein-aether scalar-tensor model in the noncommutative phase space, and compare the results with other theories mentioned in the literature. One of the theories that have led to the most important challenges in cosmology so far is called Einstein's theory of general relativity, which has undergone generalizations and modifications [7]. Among these modifications, which have exciting features and results, are modifications of the renormalizability of quantum field theory, which somehow encounters a particular framework that we discuss in this article, called noncommutative space-time. Noncommutative phase space has been addressed in various theories of cosmology, and its various cosmological applications to different theories and frameworks have been discussed. The results have been compared with the latest observable data. You can see for further study in [8]. In many calculations, the effects of noncommutative parameters have been studied in various types of cosmological theories such as power-law inflation, measurement of CMB, etc. [9]. Researchers have recently studied the effects of noncommutative parameters on the inflation scenario of constant rolling in the face of various structures such as fermion systems, modified Brans-Dicke cosmology, and other cosmological forms; results are compared with the latest observable data [10]. The constant-roll inflation scenario has also been of great interest to researchers recently. In this theory, instead of using slow-rolling formalism for inflationary studies, they use a particular condition called the constant-roll condition, which

challenges inflation scenarios and provides analytical and accurate answers for some cosmological parameters such as the Hubble parameter, potential, scale factor, and so on. This theory has been widely discussed in the literature. Such a condition has challenged various structures of effective theories such as low energy effective theory,  $f(R)$  gravity, and other modified gravitational theories. The results with the latest observational data and accepted and other theories in the literature have yielded exciting results. Some of these works can be found in [11].

## The Model

Recently, different types of Einstein-aether cosmological models with the scalar fields have been introduced, and some work has been done in this field in the literature [12]. Among them, the potential of a scalar field for the quintessence field is assumed as a function of specific aether field variables, and its structures are challenged, which has been studied as a general and basic model. Kanno and Soda [13] with the introduction of specific Lagrange, attracted the attention of the scientific community. They introduced an integral action concerning the Einstein-aether coupling parameters, a scalar field function. Such a study led to the fact that this cosmic model experiences two periods of inflation. When the scalar field is dominant, we will have a slow-roll era, and when the aether field contributes to the cosmological fluid, the Lorentz violating state will be established. With respect to [13] the results were presented, including the dynamics of the chaotic inflationary model. The interpretations were used to introduce toy models to study structures such as the Lorentz violating DGP model with no ghosts [14]. The above model has been extensively studied in the literature by researchers, and its various cosmological applications have been investigated, among which you can see in [14]. The Lorentz violating study has also been studied to analyze cosmological histories and cosmological observations and found that Einstein-aether cosmology can be used to describe cosmological observations [15]. Meanwhile, the study of the dynamics models by aether field has been the subject of work of many researchers, and a lot of work has been done that for further research you can see [16,17,18,19,20]. Some researchers have also studied Einstein-aether scalar field cosmology using exact symmetry analysis. Among the most important work done by researchers in recent years, that have quantized in Einstein-aether scalar field cosmology. Using the descriptions detailed in [13] It is discussed that the generalization of the gravitational model can be considered and a scalar field assumed in the Jordan framework, i.e., a scalar field that is coupled with the gravitational section. The Einstein-aether scalar-tensor gravitational model can be considered an integral action as  $S = S_{ST} + S_{aether}$ , Where defined as;

$$S_{ST} = \int d^4x \sqrt{-g} [ F(\phi)R + g^{\mu\nu}\phi_{;\mu}\phi_{;\nu} / 2 + V(\phi) ] \quad (1)$$

$$S_{aether} = - \int d^4x \sqrt{-g} [ \beta_1(\phi)U^{;\mu}U_{;\mu} + \beta_2(\phi)(g^{\mu\nu}U_{;\mu;\nu})^2 + \beta_3(\phi)U^{;\mu}U_{;\mu;\nu} + \beta_4(\phi)U^\mu U^\nu U_{;\mu}U_{;\nu} - \lambda(U^\mu U_\mu + 1) ] \quad (2)$$

In the above equation, we have a series of parameters such as  $\beta_1$ ,  $\beta_2$ ,  $\beta_3$ , and  $\beta_4$  coefficient functions which describe the coupling between the aether field and the scalar field, and ( $\lambda$ ) Lagrange multiplier, which specifies the unitarian of the aether field ( $U^\mu U_\mu + 1 = 0$ ). Also, the homogeneous and isotropic universe is described using the FLRW flat metric according to the cosmological structures, which is mentioned as  $ds^2 = -N^2(t)dt^2 + a^2(t)[dx^2+dy^2+dz^2]$ , Here,  $N(t)$  and  $a(t)$  specify the lapse function and scale factor, respectively, which can explain the three-dimensional radius of the Euclidean space.

According to the above explanations and equations, the Lagrangian point-like equation of the mentioned model, which can describe the field equations, is written in the following form;

$$L(N, a, da/dt, \phi, d\phi/dt) = 1/N [ 6A(\phi)a(da/dt)^2 + 6B(\phi)a^2 (da/dt)^2 d\phi/dt + 1/2 a^3 (d\phi/dt)^2 ] - N a^3 V(\phi) \quad (3)$$

## 3 Noncommutative phase space

Since Einstein's theory of gravitation is not suitable for explaining the structures of the universe at very high energies, researchers have proposed alternatives that result from the modification or expression of theories with new systems. In this regard, various theories and formulations can be mentioned, including the structure Snyder [7,8] Which describes a specific set of the NC spacetime coordinates. This structure introduces a short-length cutoff called the noncommutative parameter, which can modify features such as renormalizability properties of relativistic quantum field theory. [7,8]. NC effects can be significant when dealing with scales where the effects of quantum gravity are substantial. Since the problem of cosmological inflation at such energy scales has significant challenges, the use of such deformed phase space scenarios at these scales seems appropriate to study such a dynamic phase of the universe. In general, such a structure of spacetime has recently been considered by researchers, and many of its cosmological applications have been studied and compared with the latest observable data as well as other works in the literature. For example, clearly in [21] NC spacetime affected on power-law inflation has been investigated and showed a specific function of running the spectra index. We obtain here a specific type of these achievements, which is a particular type of canonical noncommutativity using an appropriate deformation on the classical phase space variables. One of the most important relations that we will benefit from in the calculations is the deformed Poisson bracket between the canonical conjugate moment, expressed as  $\{P_a, P_\phi\} = \theta\phi^3$ . We can also apply the following formulas in our calculations.  $\{P_a, f(P_a, P_\phi)\} = \theta\phi^3 \partial f / \partial P_\phi$  and  $\{P_\phi, f(P_a, P_\phi)\} = -\theta\phi^3 \partial f / \partial P_a$ . By tending the parameter ( $\theta$ ) to zero, all the above equations are recovered to standard commutative equations. From this relation, the Hamiltonian is calculated as follows;

$$H = 1/N [ P_\phi^2 / 2a^3 + 846a^5 (A - 3B^2)^3 / (aP_a - 6B P_\phi)^2 + Na^3 V(\phi) ] \quad (4)$$

we calculate the equations as follows;

$$da/dt = \{a, H\} = 1/N [ 864a^5 (A - 3B^2)^3 (2 aP_a - 12 aB P_\phi)^{-1} ] \quad (5)$$

$$d\phi/dt = 1/N [ P_\phi a^3 + 864a^5 (A - 3B^2)^3 (-12 aB P_\phi + 36B)^{-1} ] \quad (6)$$

$$dP_a/dt = 1/N [ 3P_\phi^2 / 2a^4 + \theta\phi^3 / a^3 P_\phi - 864(A - 3B^2)^3 5a^4 / (aP_a - 6BP_\phi) + 864a^5 (A - 3B^2)^3 (-2aP_a^2 + 12 P_a P_\phi - 12aB P_a \theta\phi^3 + 36B \theta\phi^3)^{-1} ] \quad (7)$$

$$dP_\phi/dt = 1/N [ 864a^5 / (aP_a - 6BP_\phi)^2 - 3A^2 A' + 18A^2 B B' - 108AB^3 B' - 27A'B^4 + 162B^5 B' + 864a^5 (A - 3B^2)^3 (-2a^2 \theta\phi^3 P_a + 12aB' P_a P_\phi + 12aBP_\phi \theta\phi^3 - 36B' P_\phi)^{-1} ] + Na^3 V'(\phi) \quad (8)$$

Now according to the above equations, and  $dPN/dt = P_\phi^2 / 2a^3 N^2 + (846a^5 (A - 3B^2)^3 / (aP_a - 6BP_\phi)^2 N^2) - a^3 V(\phi)$  with respect to  $N=1$ , we can calculate the Einstein-æther scalar-tensor cosmology equations in the non-commutativity phase space in the following form;

$$3[(da/dt)/a]^2 = 8\pi G(d\phi/dt / 2 + V) \quad (9)$$

$$[(d^2a/dt^2)/a] + 2[(da/dt)/a]^2 = -8\pi G[d\phi/dt / 2 - V + 216(A - 3B^2)^3 \theta\phi^3 / (A^2 A' + B^2 B')] \quad (10)$$

we use equations (9) and (10); in this case, we will have;

$$[(d^2a/dt^2)/a] - [(da/dt)/a]^2 = -(d\phi/dt)^2 - 216(A - 3B^2)^3 \theta\phi^3 / (A^2 A' + B^2 B') \quad (11)$$

Here we use the Hubble parameter definition  $H = (da/dt) / a$  and rewrite equation (11) as follows;

$$dH/dt = -(d\phi/dt)^2 - 216(A - 3B^2)^3 \theta\phi^3 / (A^2 A' + B^2 B') \quad (12)$$

We can calculate the parameter  $d\phi/dt$  as follows using a straightforward calculation with respect to

$$dH/dt = (dH/d\phi) d\phi/dt;$$

$$d\phi/dt = -1/2 dH/d\phi \pm 1/2 [(dH/d\phi)^2 - 864(A - 3B^2)^3 \theta\phi^3 / (A^2 A' + B^2 B')]^{1/2} \quad (13)$$

We derivative from the above equation, and the relation used in the constant-roll inflation scenario such as  $(d^2\phi/dt^2) = -(3 + \alpha)H\dot{\phi}$ , we will have;

$$-(3 + \alpha)H = -1/2 d^2H/d\phi^2 \pm [ d^2H/d\phi^2 dH/d\phi - ((864[ 3A^2 A' - 18AA'B^2 - 18BB'A^2 + 27B^4 + 108AB'B^3 - 162B'B^5] \theta\phi^3 \times 3\theta\phi^2 (A - 3B^2)^3) \times (A^2 A' + B^2 B') - 864(A - 3B^2)^3 \theta\phi^3 (A''A^2 + 2AA'^2 + 2BB'^2 + B^2 B'') ) / (2[(dH/d\phi)^2 - 864(A - 3B^2)^3 \theta\phi^3 / (A^2 A' + B^2 B')]^{1/2} ] \quad (14)$$

if we consider parameters such as  $(\theta)$ ,  $A$ , and  $B$  as zero, equation (14) becomes an ordinary equation in the literature. In fact, in this case, equation (14) becomes two equations, one zero and the other becomes the following form.  $d^2H/d\phi^2 - (3 + \alpha)H = 0$ . The above equation is an ordinary differential equation whose answer will be calculated as follows;

$$H = c_1 \exp(\sqrt{3 + \alpha}) + c_2 \exp(-\sqrt{3 + \alpha}) \quad (15)$$

Now we have to assume a particular ansatz to solve the whole equation (22) that contains essential parameters such as  $(\theta)$ ,  $A$ , and  $B$  so that the consequence of these parameters on significant quantities and parameters such as Hubble parameter and potential can be investigated. Hence we will have;

$$H = c_1 \exp(\lambda(\theta, A, B) \sqrt{3 + \alpha}) + c_2 \exp(-\lambda(\theta, A, B) \sqrt{3 + \alpha}) \quad (16)$$

The parameter  $(\lambda)$  can be calculated directly by placing (25) in the equation (22). By calculating this parameter  $(\lambda)$  and placing it in equation (25), we can calculate the explicit relationship for the Hubble parameter according to different boundary conditions. Then we can use it to calculate other quantities such as Hubble parameter. In this way, we can have the Hubble parameter by creating the appropriate boundary conditions. By calculating the Hubble parameter, all other important quantities such as potential, scale factor and velocity field  $(d\phi/dt)$  and other quantities considered in the inflation scenario can be quickly investigated. Therefore, in the continuation of the article, we assume two boundary conditions and calculate the Hubble parameter appropriate to each boundary condition. Finally, we summarize the results of our work. Due to the large of potential sentences  $V$ , etc., their calculation is ignored. Therefore, we know that other desired quantities can be quickly and directly calculated by investigating a Hubble parameter. we apply the first boundary condition  $(c_1 = c_2 = M/2)$  to equation (16). In the following, different answers are obtained for the Hubble parameter, in which we consider only the positive solution. Therefore, according to the concepts mentioned earlier, the Hubble parameter is calculated according to the first boundary condition in the following form;

$$X = 3\sqrt{3} [ 2(3 + \alpha)^{3/2} (-3 + \sqrt{3}\phi + \sqrt{3 + \alpha})^2 (A''A^2 + B^2B'' + 2AA'^2 + 2BB'^2) / (27\sqrt{3} 3B^4B' + AA'' + 2AA'B^2 + 64AB''B^3) - \phi^2 (3A^2A' + 18AA'B^2\phi - 162B'B^5\phi + 9B'(-2 + 3B' + 2B'\phi))\theta / (A^2A' + B^2B')^2 + 864(A - 3B^2)^3 \theta\phi^3 (2AA'^2 + B(2B'^2 + BB')) + A^2A' / (A^2A' + B^2B')^4 ],$$

$$Y = 2(M^2\phi^2 (3 + \alpha)^2 (-6 - \alpha + 2\sqrt{3}\sqrt{3 + \alpha})),$$

$$H = M \cosh [ \phi ( M(3 + \alpha) - X/Y ) / 2\sqrt{3}\sqrt{3 + \alpha}(M + M\sqrt{3 + \alpha}/\sqrt{3}) ]. \quad (17)$$

Now, using the above equation, we can calculate the potential for the first case, and another important parameter, i.e.,  $(d\phi/dt)$ . other quantities such as scale factor can be calculated according to the definition of the Hubble parameter. In the continuation of this article, we apply the same calculations for the second boundary condition. We apply the second boundary condition  $(c_1 = M/2, c_2 = -M/2)$  to equation (16). Hence the Hubble parameter is calculated according to the second boundary condition as follow;

$$O = 27\theta\phi [ (A^2A' + B^2B') (162A^2 + 18AA'\phi - 6AB^2 + 9B'(-2AA' - 12ABB' + 3B' + 36B'B^5)) - 864(A + 3B^2)^3\phi + 2B'\phi(2AA'^2 + B(2B'^2 + BB')) + A^2A'' + (A^2A'' + 18AA' + B^2B''\phi) \times (-3AA'(-3 + \alpha)\phi),$$

$$S = M\sqrt{3 + \alpha}\sqrt{M^2(3 + \alpha)(-3 + \phi^2(3 + \alpha))(A^2A' + B^2B')^4},$$

$$H = M \sinh [ \phi ( (3 + \alpha) + \sqrt{162M/\sqrt{M^2(3 + \alpha)(-3 + \phi^2(3 + \alpha)) - O/S}} ) / 12\sqrt{3}\sqrt{3 + \alpha} ]. \quad (18)$$

Also, according to the previous subsection, each of the parameters and quantities such as potential and  $d\phi/dt$  and other quantities such as scale factor for this case can be calculated.

## Concluding remarks

In this paper, the primary purpose of this study was to investigate the constant-roll inflationary scenario with anisotropic conditions concerning the Einstein-æther Scalar-tensor Cosmology in noncommutative phase space. That is, we first introduced an Einstein-æther scalar-tensor cosmological model. In this structure, in action integral of scalar-tensor, one is introduced æther field with æther coefficients that it be a function of the scalar field, which is, in fact, a kind of extender of the previous Lorentz-violating theories. Hence, we presented the point-like Lagrangian, which represents the equations of the Einstein-æther Scalar-tensor model. Then we calculated the Hamiltonian of our model directly. According to the noncommutative phase space characteristics, we obtained the some equations of this model. In the

following, according to the constant-roll conditions, we studied the anisotropic constant-roll inflationary scenario and calculated some cosmological parameters of the mentioned model, such as the Hubble parameter, potential, etc. The findings of the mentioned paper can be extended to other scalar-tensor theories and challenge their cosmological applications. The model mentioned in this paper or other models can also examine the scalar-tensor cosmology in different contexts and compare the results. The findings of this article can be challenged with a new idea that has recently been very much of interest to researchers, namely to the swampland program, and compare the results with the latest observable data. It is also possible to study different theories of cosmology in the noncommutative phase space and select the best models among them that are most consistent with the latest observable data. Also, examining different types of cosmological models with such a proposed structure provided in this paper can propose a new classification for cosmological models.

## References

- [1] D. Mattingly, “Living Reviews in Relativity”, ApJ, 8, 5, 20 (2005).
- [2] A. Kostelecky, “Gravity, Lorentz violation, and the standard model”, Phys. Rev. D 69, 105009 (2004).
- [3] S.M. Carroll, H. Tam and I.K. Wehus, “Lorentz violation in Goldstone gravity”, Phys. Rev. D 80, 025020 (2009).
- [4] T. Jacobson, “Extended Hořava gravity and Einstein-aether theory”, Phys. Rev. D 81, 10502 (2010).
- [5] C. Eling, T. Jacobson and M.C. Miller, “Neutron stars in Einstein-aether theory”, Phys. Rev. D. 76, 042003 (2007).
- [6] T.P. Sotiriou, M. Visser and S. Weinfurter, “Phenomenologically viable Lorentz violating quantum gravity”, Phys. Rev. Lett. 102, 251601 (2009).
- [7] H. S. Snyder, “Quantized space-time”, Phys. Rev. 71, 38 (1947).
- [8] H. S. Snyder, “The electromagnetic field in quantized space-time”, Phys. Rev. 72, 68 (1947).
- [9] Q. C. Huang, and M. Li, “Power spectra in spacetime noncommutative inflation”, Nucl. Phys. B713, 219 (2005).
- [10] J. Sadeghi, S. Noori Gashti, “Anisotropic constant-roll inflation with noncommutative model and swampland conjectures”, Eur. Phys. J. C 81, 301 (2021).
- [11] H. Motohashi, and A. A. Starobinsky, “Constant-roll inflation: confrontation with recent observational data”, EPL 117 (2017).
- [12] W. Donnelly and T. Jacobson, “Coupling the inflaton to an expanding aether”, Phys. Rev. D 82, 064032 (2010).
- [13] S. Kanno and J. Soda, “Lorentz violating inflation”, Phys. Rev. D 74, 063505 (2006).
- [14] T. Kaneshima, P. Channuie and N. Kaewkhao, “Noether symmetry approach in Eddington-inspired Born–Infeld gravity”, EPJC 81, 357 (2021).
- [15] J.A. Zuntz, P.G. Ferreira and T.G. Zlosnik, “Constraining Lorentz violation with cosmology”, Phys. Rev. Lett. 101, 261102 (2008).
- [16] Arianto, F.P. Zen, Triyanta and B.E. Gunara, “Attractor solutions in Lorentz violating scalar-vector-tensor theory”, Phys. Rev. D 77, 123517 (2008).
- [17] A. Paliathanasis, G. Papagiannopoulos, S. Basilakos and J.D. Barrow, “Dynamics of Einstein–Aether scalar field cosmology”, EPJC 79, 723 (2019). 21
- [18] A. Paliathanasis, “Extended analysis for the Evolution of the Cosmological history in Einstein-aether Scalar Field theory”, Phys. Rev. D 101, 064008 (2020).
- [19] A. Paliathanasis and G. Leon, “Integrability and cosmological solutions in Einstein-aether-Weyl theory”, EPJC 81, 255 (2021).
- [20] A. Paliathanasis and G. Leon, “Analytic solutions in Einstein-aether scalar field cosmology” EPJC 80, 355 (2020).
- [21] S. M. M. Rasouli, A.H. Ziaie, J. Marto and P.M. Moniz, “Gravitational collapse of a homogeneous scalar field in deformed phase space”, Phys. Rev. D 89, 044028 (2014).

## Color Reconnection Modelling in PYTHIA8

Nameeqa Firdous<sup>1</sup>, Malik Junaid<sup>2</sup>

<sup>1</sup>GIFT University Gujranwala Pakistan

<sup>2</sup>University of Innsbruck, Innsbruck Austria

**Abstract:** Color reconnection (CR) is a mechanism needed to describe the high energy hadronic interactions that can occur between color fields during the process of hadronization i.e., formation of colourless hadrons out of colored quarks and gluons. It is essential to describe the increase of the average transverse momentum as a function of charged particle multiplicity; it is observed that multiplicity dependent event shape data is also sensitive to the CR mechanism. In this study, two different methods implemented in PYTHIA8 Monte Carlo event generator were investigated along with no color reconnection option. In the first model, the color flow is reconstructed by how a parton shower could have constructed the configuration. In the second model, the full QCD color calculation is taken into account. It is clearly shown that selected observables cannot be described well without CR. Simulation results were compared with LHC data.

### Introduction

Simulation of a high energy collision event is a complicated process, which requires a systematic understanding of multi-particle production processes. It includes many physics processes like, hard processes involving large momentum transfer, parton distribution functions, multiple parton interactions (MPIs), initial-state radiation (ISR), final-state radiation (FSR), beam Remnants, hadronization and decays. All of these physics processes pose their own challenges, but are understandable to a large extent when treated individually. When combined, additional sources of uncertainty appear, however. Foremost among these, colour reconnection (CR) represents the uncertainty induced by the high density of colour charges that may interact in a nontrivial nonlinear manner.

Color reconnection [2,3,4] mechanism was introduced in PYTHIA [1], in an attempt to explain the increase in average transverse momentum vs charged multiplicity as observed by UA1 experimental data. The starting point here is that large charged particle multiplicities predominantly come from having a large Multiparton Interaction (MPI) activity, rather than from high transverse momentum jets. If each such MPI produces particles more-or-less independently of each other, then the average transverse momentum should be independent of the number of MPIs, and hence of multiplicity. The alternative is that each further MPI brings less and less additional multiplicity, while still providing an equally big transverse momentum kick from the semi-hard interaction itself, to be shared among the produced hadrons.

### Methodology

Because of the composite nature of hadrons, there are more than one parton-parton interactions that occur in a single hadron hadron collision, known as Multiparton interaction (MPI). It is well known that the systematic understanding of multi-particle production processes is out of reach at the moment. So to confront the experimental data with theoretical predictions approximate solutions, such as simulation programs are used called event generators or QCD Models. These event generators decompose the full scattering process into a sequence of different stages, which are usually characterised by different energy scales.

This property turns event generators into the perfect tool to be used. In this study we use the PHYTHA 8 Monte Carlo event generator.

In this QCD model colour flows in the separate sub processes defined in the multiparton interactions scenario are tied together via the assignment of colour flow in the beam remnant.

Fours models are implemented in PYHTIA8 to include the color reconnection effects, two were studied in this paper. In PYTHIA8 different models were as below:

flag ColourReconnection:reconnect (default = on)

mode ColourReconnection:mode (default = 0; minimum = 0; maximum = 4)

Determine which model is used for colour reconnection.

option 0 : The MPI-based original Pythia 8 scheme.

option 1 : The new more QCD based scheme. Should be combined with BeamRemnants:remnantMode = 1.

option 2 : The new gluon-move model, wherein gluons can be moved from one location to another so as to reduce the total string length. This is one out of a range of simple models developed to study potential colour reconnection effects e.g. on top mass

## Results and Discussion

We considered four different CR treatments implemented in PYTHIA 8 including no CR at all. The transverse momentum distribution and average transverse momentum vs multiplicity ( $N_{ch}$ ), shown in Figure 3 appears to be sensitive to the color structure of the events, within the framework of the PYTHIA8 modelling. Transverse momentum ( $p_t$ ) distribution is badly described and average transverse momentum shows quite a soft spectrum when CR is switched off. It is clear from MC/data comparison plots in Figure 2 that to describe data color reconnection model should be switched on. The remaining three model choices describe data equally well except at the higher transverse momentum tail where the first choice seems better than the other choice It is also noted that the option CR 2 needs more studies for the better understanding of its behaviour. CR is necessary not only to describe average  $p_t$  vs multiplicity but also the eta distribution ( $dn_{ch}/d\eta$ ) as shown in Figure 1.

## Conclusion

Different options of CR mechanism offered by PYTHIA8 are investigated using ATLAS Minimum Bias data at 0.9 and 7TeV [5]. To study CR mechanism, the multiparton interaction model should be switched on to get reasonable results for hadron-hadron collision data. It is clear from MC/data comparison that without the color reconnection model the transverse momentum spectrum is too soft. The other three options for the CR model do not show significant differences in the predictions.

All plots are produced using Rivet toolkit [6].

## References

1. T. Sjöstrand, S. Mrenna and P. Skands, A brief introduction to PYTHIA 8.1, *Comput. Phys. Commun.* 178 (2008) 852.
2. J. R. Christiansen and P. Z. Skands, String Formation Beyond Leading Colour, *JHEP* 08 (2015) 003, arXiv: 1505.01681 [hep-ph].
3. S. Argyropoulos and T. Sjöstrand, Effects of color reconnection on tt final states at the LHC, *JHEP* 11 (2014) 043, arXiv: 1407.6653 [hep-ph].
4. J. R. Christiansen and T. Sjöstrand, Color reconnection at future  $e^+e^-$  colliders, *Eur. Phys. J. C* 75 (2015) 441, arXiv: 1506.09085 [hep-ph].
5. G. Aad et al. Charged-particle multiplicities in pp interactions measured with the ATLAS detector at the LHC. *New J.Phys.*, 13:053033, 2011.
6. A. Buckley et al., Rivet user manual, *Comput. Phys. Commun.* 184 (2013) 2803, arXiv: 1003.0694 [hep-ph].

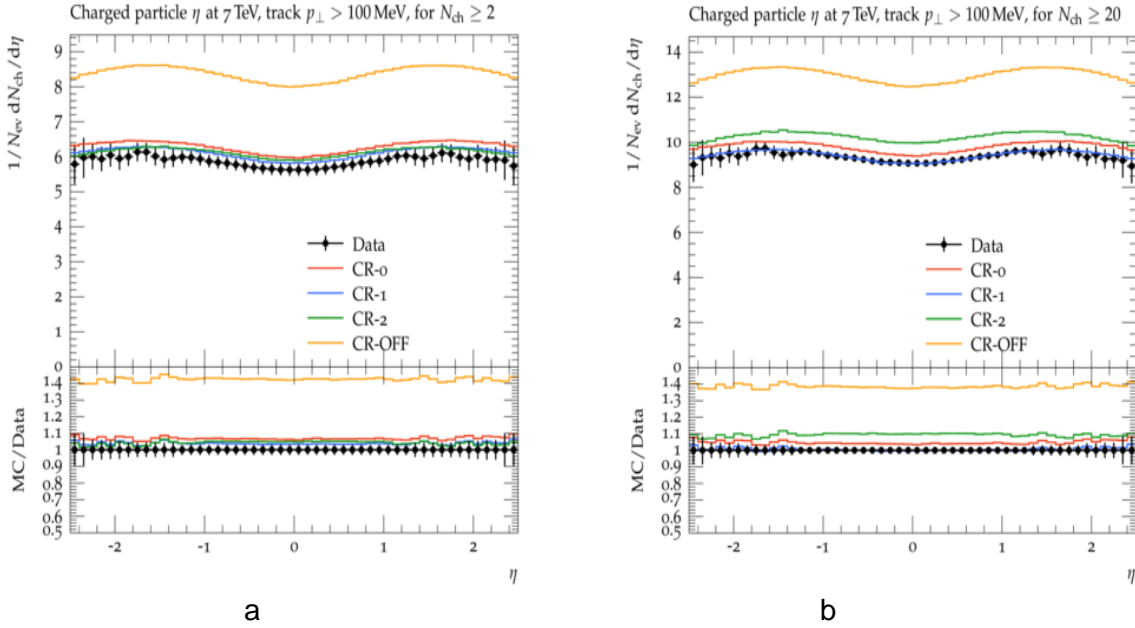


Figure 1: Comparison plots of Pythia 8 prediction to the real data from ATLAS experiment at 7.TeV :eta distribution

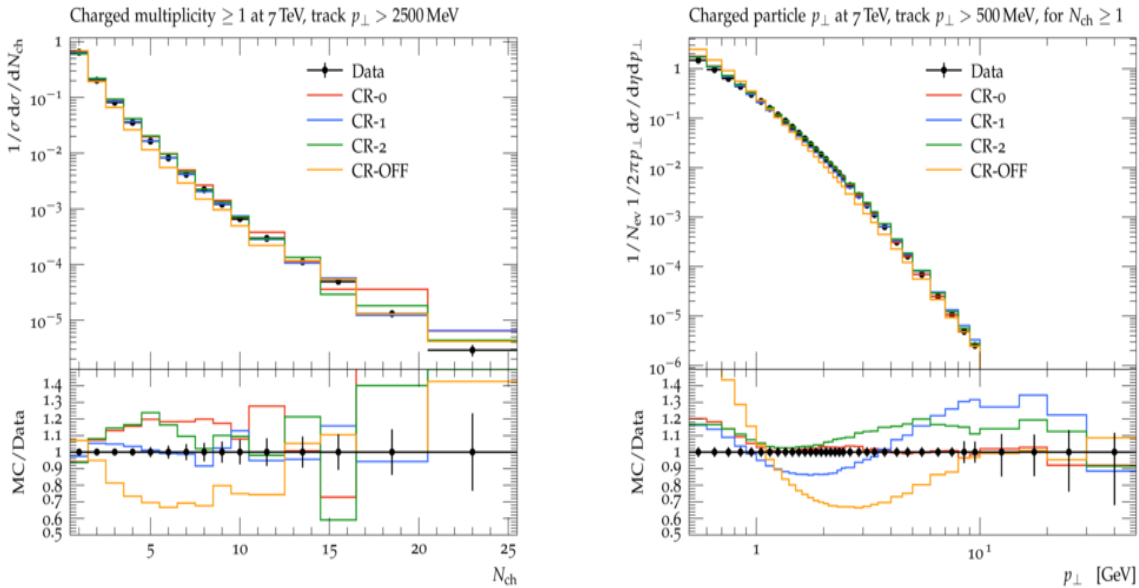


Figure 1: Comparison plots of Pythia 8 prediction to the real data from ATLAS experiment at 7.TeV (multiplicity and transverse momentum distributions)

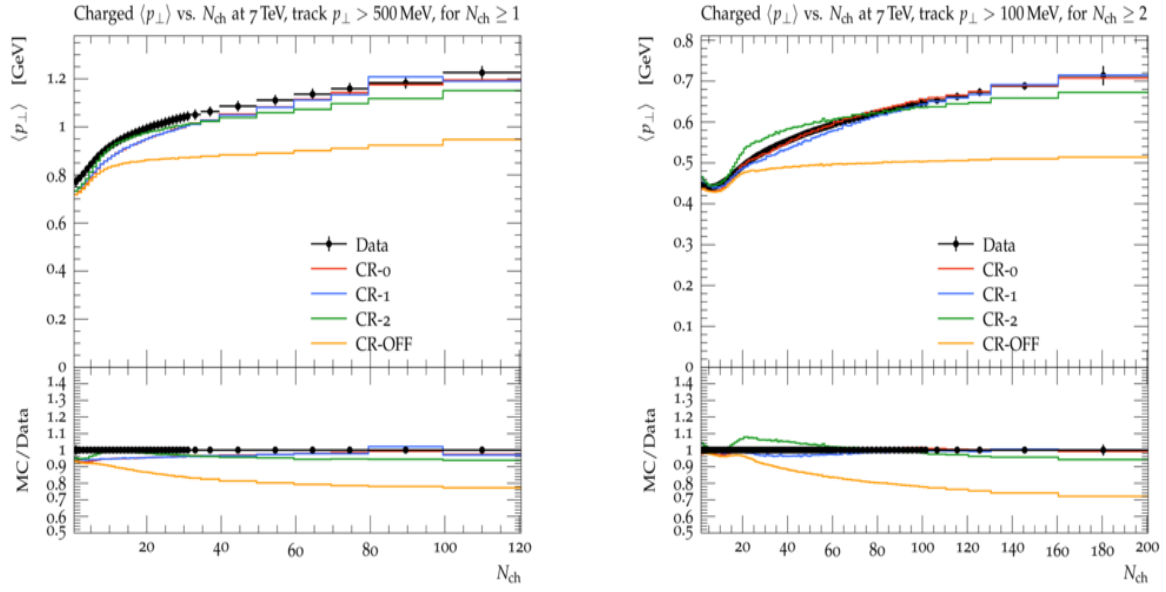


Figure 1: Comparison plots of Pythia 8 prediction to the real data from ATLAS experiment at 7.TeV: average  $p_t$  vs  $N_{ch}$  distribution